Ion-Selective All-Solid-State Printed Sensors: A Systematic Review

Giorgia Polidori, Sarah Tonello, *Member, IEE*, and Mauro Serpelloni, *Senior Member, IEEE*

***Abstract*—The recent advancements in technologies related to printed electronics brought significant innovation in the design and fabrication of electrochemical miniaturized sensors. One of the most exciting categories that can benefit from the transition from macro to micro enabled by novel printing techniques is ion-selective electrodes (ISEs). Miniaturized ISEs are also called "all-solid-state ISEs" (ASS-ISEs) since they rely on a solid contact (SC) transduction layer, enabling easier miniaturization and integration. This is particularly interesting for a wide variety of applications ranging from medical to industrial. In all these fields, printed ASS-ISEs have been proven to reach significant results in terms of metrological properties, obtaining near-Nernstian sensitivities, limits of detection down to 10^{-10}, best selectivity coefficients around 10^{-8}, shorter response time lower than 5 s, stability reaching six months and optimal variabilities (with best repeatability (RP) lower than 1% and reproducibility (RPR) lower than 2%). The use of innovative printing techniques could further enhance these properties, as well as improve aspects such as flexibility, material waste, resolution improvement, and the finest control of surface functionalization. Although a wide range of examples has multiplied in the literature over the past decade, to date, most of them still lack uniformity or detailed guidance regarding both the fabrication process and the metrological characterization procedure. With this in mind, this review aims to serve as a guideline for the identification of project specifications for the design, fabrication, and test of ion-selective ASS printed sensors, as well as to propose a common metric in characterizing these devices.**

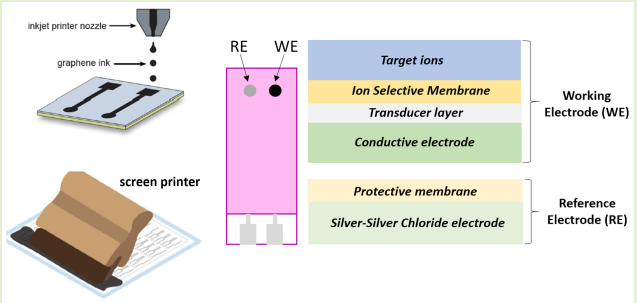

***Index Terms*— All-solid-state (ASS) sensors, drugs, ions, ion-selective membranes (ISMs), ion-selective sensors, molecular imprinted polymers (MIPs),molecules, nonmolecular imprinted polymers, printed sensors, solid-contact (SC) ion-selective electrodes (ISEs).**

I. Introduction

THE recent advancements in technologies related to printed electronics brought significant innovation in the design and fabrication of electrochemical miniaturized sensors. By printing the electrodes and tracks on selected substrates (e.g., alumina, paper, plastic), it is thus possible to reduce the size of the macroscopic traditional electrochemical cell down to a few square millimeters, with advantages in terms of reduction of material waste, the possibility of integration in complex systems and analysis of low volume samples [1].

Among the wide variety of electrochemical sensors, one of the most interesting categories that has exploited these transitions from the macro to the micro is ion-selective electrodes (ISEs) [2]. This definition encompasses all those sensors that aim to quantify ion concentration correlating it with an electrical output parameter (e.g., potential, impedance, current). This class of sensors has proven to be very interesting due to the wide range of applications, ranging from healthcare [3] to agri-food smart applications [4] or environmental monitoring [5]. With these types of sensors, one of the most widespread applications rely on ions quantification within biofluids (sweat, plasma) to monitor human health in particular in terms of hydration state, muscular exercise, and different types of diseases [6]. Research is, however, rapidly expanding to other areas, including monitoring heavy metal contamination in people exposed to high-risk environments, monitoring liver and bone status, monitoring pharmacotherapy in people with bipolar disorder, and skeletal and dental studies. Quantification of ions is also important in agriculture for monitoring water and food quality and for studying the effect of detergent production on water [7].

The main transducing principle exploited to detect ions with ISEs is based on potentiometry. Thanks to the presence of a selective membrane able to bind the charged target ions of interest next to a conductive electrode, a potential difference proportional to the ion concentration is measured

Manuscript received 7 November 2023; revised 3 January 2024 and 9 January 2024; accepted 11 January 2024. Date of publication 23 January 2024; date of current version 14 March 2024. The associate editor coordinating the review of this article and approving it for publication was Dr. Marios Sophocleous. *(Corresponding author: Giorgia Polidori.)*

Giorgia Polidori and Mauro Serpelloni are with the Department of Information Engineering, University of Brescia, 25123 Brescia, Italy (e-mail: giorgia.polidori@unibs.it).

Sarah Tonello is with the Department of Information Engineering, University of Padova, 35131 Padua, Italy.

Digital Object Identifier 10.1109/JSEN.2024.3354321

by exploiting different electrode configurations (e.g., electrochemical, transistor-based) [8].

Different approaches in terms of manufacturing within the class of ISEs are found in the literature, leading to different classifications. The first and most widespread classification refers to the physical state of the selective membrane, which allows distinguishing ISEs in glass membrane ISEs, polymeric or liquid membrane ISEs, or crystal or solid membrane ISEs [9]; furthermore, classification can also be performed depending on the presence of a liquid solution or a solid interlayer between electrodes and membrane to realize the transduction, which brings the distinction between conventional ISEs and all-solid-state ISEs (ASS-ISEs) [sometimes also defined as solid contact ISEs (SC-ISEs)] [10].

Conventional ISEs represent the most robust and well-known class of ISEs. They have a glass body and an electrolyte solution on both sides of the membrane; these systems are very accurate, with high stability and a long lifetime; however, the main drawbacks that pushed researchers to find an alternative design are, first of all, the fact that the internal electrolyte of ISEs is prone to evaporation and also sensitive to environmental parameters (e.g., temperature, pressure) possibly leading to volume changes [11]. Further, the presence of the filling solution limits the possibility of miniaturizing these systems [12].

ASS-ISEs represent the most promising evolution of conventional ISEs, where the liquid electrolyte solution has been replaced by a solid-state interlayer material, and stick electrodes have been transformed into 2-D electrodes on a flat substrate. This design evolution makes ASS-ISEs the most suitable candidates for miniaturization and integration with driver circuits and readout electronics in portable wearables or point-of-care devices [13].

Several ASS-ISE designs and operation modes have been proposed so far. A standard configuration is a two-electrode layout, with only a working electrode (WE) and a reference electrode (RE), working as an electrochemical potentiometric sensor [14]. Another configuration is the three-electrode design, adding a counter electrode (CE) to the layout [15]. As expected, the two-electrode layout ensures the miniaturization of both the sensing element and the associated simple conditioning circuit. One of the disadvantages of this layout is related to the drift and instability of the signals in very long-time monitoring. Three-electrode layouts are preferred in applications where a controlled potential should be applied (, voltammetry, amperometry-based sensors) [15]. For potentiometric sensors, where an open circuit potential (OCP) is measured without applying any external potential, a third electrode is not necessary to ensure external potential stability; thus, the two-electrode layout is sufficient to achieve sensitive ion detection, and the only important aspect is to guarantee a stable reference potential through proper RE [16]. Another configuration to the traditional two-electrode or three-electrode electrochemical design is the use of ion-sensitive FET (ISFET). The ISFET design consists of three terminals (source, drain, and gate) plus an additional RE [17]. During operation for ion detection, a gate voltage (V_{GS}) is applied by RE through an electrolyte solution, increased to a threshold voltage (V_T), which makes the channel conductive with current (I_{DS}) and voltage (V_{DS}) generated between the source and drain electrodes. Since the concentration of ions in the analytes directly affects the required V_T, ion quantification is performed directly from V_T. In spite of the high sensitivities that can be reached, any change in threshold voltage due to temperature and drift effect can limit the accuracy of the ISFET detection [17], [18], [19]. The choice of ASS-ISE design and operation mode must be driven by a trade-off between the level of miniaturization required, the need to apply external potentials, the importance of its stability, the level of expected interferences, and the simplicity of the targeted conditioning circuit. When it comes specifically to printed ASS-ISE, where rapid prototyping and process flexibility are the highest priorities, two-electrode designs are still preferred over ISFETs, which still require more complex design and manufacturing considerations to enable accurate and stable results [17]. In a two-electrode configuration, a selective membrane is always deposited on top of the WE to bind the target analyte of interest in the solution. Further, a polymeric protective membrane can be deposited on the RE to improve its function and guarantee the stability of a reference potential. The final transduction is performed by measuring the potential difference between the two electrodes that is due to the concentration of target ions bound on the WE membrane [20]. The enormous advantages of its design rely on the simplicity of the geometry and also of the conditioning circuit to measure the potential difference [21]. In recent decades, ASS-ISEs have benefited from the advantages of printing techniques. Particular attention has been paid to realize not only electrodes but also ion-to-electron interfaces and selective membranes by printing techniques [22]. The wide variety of printing techniques available, including screen printing, inkjet printing, and aerosol jet printing, can lead to different kinds of benefits for ASS-ISEs over other fabrication and deposition techniques [23], [24]. These advantages include more controlled geometries, better resolution, the possibility of control over where to deposit various components, deposition on nonconventional substrates such as papers and plastics, or printing on irregular, curved substrates or complete objects [21].

In this picture, this review aims to provide state-of-the-art ion-selective ASS printed sensors (ASS-ISEs) with a focus on printed methods and materials and metrological characteristics. This review is intended to serve as a guideline for the identification of project specifications for the design, fabrication, and test of ion-selective ASS printed sensors. A further goal is to finally propose a common metric in characterizing these devices since, comparing works in the literature dealing with printed ISEs, much dispersion and nonuniformity of the terminology can be observed.

II. Systematic Literature Review Process

The review took into consideration original studies identified on one different online database, Scopus, and published from 2013 to 2023.

The search was performed on title, abstract, and keyword by using the following string: (electrodes OR sensors) AND

(printed OR printing) AND ((ion AND selective) OR ISE) AND (selectivity OR sensitivity OR "limit of detection") OR LOD OR stability) AND ((conductive AND polymers) OR nanostructures OR microstructures OR graphene OR nanotubes OR PEDOT) AND (potentiometric OR potentiometry). This string was specifically designed to include only complete works that consider not only fabrication but also a complete characterization of the ASS-ISEs.

The performed literature research identified 45 articles. Of these articles, only 36 were finally considered after an evaluation of the manufacturing methods, transduction technique, and completeness of the metrological characteristics. These articles were analyzed, and the following details were extracted, compared, and discussed through the text and summarized in the cumulative tables reported at the end of the article. Particular attention was given to applications (target ions); electrode material and printing techniques; ion-to-electron transducing materials and deposition techniques; type of membranes; type of transducing principle (predominantly potentiometric); electronics design; metrological features, including sensitivity, limit of detection (LOD), selectivity, repeatability (RP), reproducibility (RPR), stability, response time, and lifetime.

III. Working Principle of ASS-ISEs

In spite of a wide variety of differences in materials, applications, and fabrication techniques exploited in the examples in the literature, ASS-ISEs have a common design structure. The most employed layout is a two-electrode layout with a WE and RE. The WE is always functionalized with an ion-selective membrane (ISM) that has the function of selectively binding target ions in the solution under test and keeping them near the WE conductive surface that enables reading changes in the potential concerning the RE. The RE should maintain a stable potential, to avoid drifting over time that can strongly modify the calibration curve of the device. This stability is often achieved by covering the electrode made of a stable and inert metal with a protecting porous membrane that freely enables the exchange of ions, usually made of polyvinyl butyral (PVB) as highlighted in most of [25], [26], [27], [28], [29], [30], [31], [32], and [33].

The measurement of the OCP of the WE concerning the RE can be correlated with the concentration of the target ion in the solution. From an analytical perspective, the transduction mechanism is based on the Nernst equation (1) that rules the electrochemical equilibrium at the interface between the aqueous solution containing the target analyte and the inner part of the ISM

$$E = \frac{RT}{Z_I F} \ln \frac{[I]_{\text{aq}}}{[I]_{\text{ISE}}} \tag{1}$$

where R is the gas constant, T is the temperature, Z_I is the valence of the target ion I, F is Faraday's constant, $[I]_{\text{aq}}$ is the unknown concentration of the target analyte, and $[I]_{\text{ISE}}$ is the concentration of the ion in the ISM.

Knowing $[I]_{\text{ISE}}$ and turning natural logarithm in base 10 log, we can obtain the following equation that indicates a linear relationship exists between the measured potential and the log of the ion concentration, as in the following equation:

$$E = 2.3 \frac{RT}{Z_I F} \log I_{\text{aq}} + \text{const.} \tag{2}$$

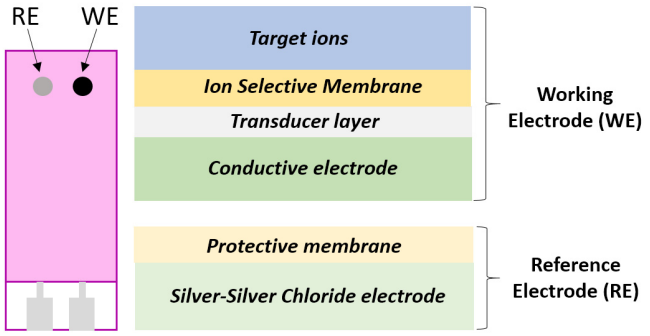

Fig. 1. Schematic layout of a typical ASS ion selective sensor (ASS-ISE).

The initial concentration of target ion in the ISM (I_{ISE}) can be modified through a specific procedure known as preconditioning of the membrane, obtained by soaking the ISM-coated electrode in a solution with a known target analyte concentration before the first use or after long-time storage. This preconditioning can strongly affect the sensitivity and the LOD of the ISEs and thus should be selected depending on the required working range.

To allow proper sensitivity, as can be seen in Fig. 1, the WE design typically features a stacked structure with the three essential layers, where the layer referred to as the "transducer layer," "interlayer," or "ion-to-electrode-interface" is interposed between the conductive electrode and the ISM. While the function of the conductive electrode is to guarantee communication with the read-out circuit, the conductive interlayer serves to improve the transduction from ions accumulated in the membrane to the electrons read by the read-out circuit.

In the following paragraph, the three layers previously reported are deeply analyzed in terms of fabrication methods and materials.

IV. Design and Materials Components in Printed ASS-ISEs

A. Electrodes: Fabrication, Design and Process Details

The first elements that must be effectively printed to guarantee an effective transmission of the signal generated from the ion-to-electron transduction are conductive, stable, long-lasting electrodes. Focusing on the printed approach involves a suitable choice of inks, substrates, and their compatibility, as well as the choice of the most suitable technique and specific printing protocol. As mentioned above, ion-selective sensors employ two electrodes, RE and WE. It has been seen in the literature that the RE is always printed using Ag/AgCl. The WE, on the other hand, can be printed with different inks, depending on different needs. Of these, carbon is the most widely used ink [25], [26], [34], [35], [36], [37], [38], [39], [40], [41], [42], [43], [44], [45], [46], [47], [48], [49], [50], [51], [52], [53], [54], [55], [56]. Different forms of carbon are used in a smaller percentage, such as

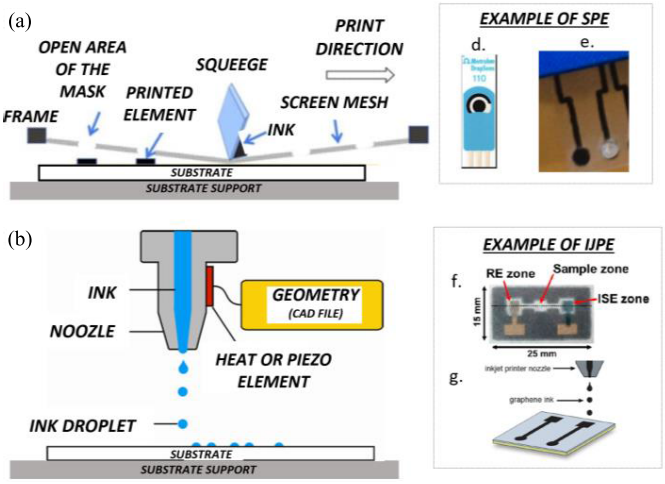

Fig. 2. Summary of the techniques exploited in the analyzed literature to realize the electrodes in ASS-ISEs: schematic reproduction of the mechanisms for (a) screen and (b) inkjet printing; examples of (c) most frequently employed commercially available SPE [26], (d) customized screen-printing (SP) ASS-ISE [33], (e) customized IJP ASS-ISE [58], and (f) [59].

carbon nanotubes (CNTs), which can be in both multiwalled CNTs (MWCNTs) and single wall (SWCNTs) forms [27], [28], [33], [57], and graphene [58]. Other printed materials may include gold [30], [31], [32] and silver [59]. In 2021, Abd-Rabboh et al. [29] constructed a potentiometric cell by incorporating a polymer membrane sulfite ISE based on cobalt(II) phthalocyanine (CoPC) as the recognition material and an Ag/AgCl RE.

As can be seen from Table I, there is a difference between carbon, graphene, and CNTs: in graphene, the carbon atoms are arranged in a hexagonal shape, while in CNTs, the carbon atoms compose ordered structures of spherical shape, in which can be coiled on itself (SWCNT) or form multiple structures coaxially coiled on each other (MWCNT). Two main printing techniques are used for the fabrication of the electrodes, as shown in Table I and Fig. 2: screen printing and inkjet printing. The advantages of these techniques for electrode fabrication have been extensively reviewed in several works [60], [61], in particular in terms of ease of operation, rapid processing, and high throughput for screen printing and process flexibility, geometry control, and reduced ink waste for inkjet printing. Screen printing is the most widely used for ASS-ISEs, as can be seen from the references in Table I. The latter is a technique that allows printing on any substrate or flat surface, and through some pressure, ink is pushed onto the printing surface. Screen-printed electrodes (SPEs) are highly exploited because they offer easy-to-use analytical methods that can be employed without the need for sophisticated equipment. Another technique that is reported in the literature is inkjet printing. He et al. [58], Ruecha et al. [59], and Garland et al. [84] printed the sensors by inkjet printing, which uses ink droplets that are pushed onto the substrates of interest.

A lack of information regarding the curing and process specification for the printing phase of the conductive electrodes could be observed. This is mainly due to the fact that a high number of works fabricating SC-ISEs are actually working on

TABLE I
DIFFERENT TYPES OF WES WITH MATERIAL DIFFERENCES, PRINTING TECHNIQUES, CURING METHODS, CURING PARAMETERS, AND POST-PROCESSING

Working Electrode	Printing technique	Curing Method	Curing parameters	Ref
Carbon	screen-printing	Heat	10 min at 70°C	[25]
			150°C	[26]
			2 h at 60°C	[35]
			30 min at 50°C	[41]
			2 h at 60°C	[43]
			150°C	[44]
			15 min at 120°C	[47]
			150°C	[48]
			15 min at 150°C	[49]
			150°C	[50]
			3 h at 60°C	[52]
			30 min at 50°C	[55]
			12 min at 80°C	[62]
		Air Drying	3 h at RT	[51]
Carbon + CNTs	screen-printing	Heat	150°C	[29]
			10 min at 70°C	[33]
			30 min at 50◦C	[57]
Gold	screen-printing	Heat	250°C	[31]
Graphene	inkjet-printed	Heat furnace	1 h at 650°C	[58]
Silver	inkjet-printed	Heat	120°C	[59]

the layers regarding the transducing layer and the selective membrane rather than on the fabrication of the electrode itself, relying on commercially available SPEs as a starting point [34], [36], [37], [38], [39], [40], [53], [54], [56].

B. Ion-to-Electron Transducing Materials

An interface material is usually printed between the electrodes and the ISM, which allows ionic and electronic interaction between the various materials used. The most commonly used deposition technique for various interface materials is drop-casting [25], [26], [28], [29], [30], [31], [32], [34], [35], [36], [37], [38], [39], [40], [41], [42], [43], [44], [46], [48], [49], [52], [53], [54], [55], [56], [58], [59]. This technique is simple, easy, and quick [63]. In addition to this technique, the interface material is often directly screen-printed using an ink obtained by mixing the electrode material with the interface layer used for the WE [33], [45], [47]; furthermore, some authors propose new and innovative manufacturing methods. Some research groups tend to electrochemically deposit the interface material [57], [62], while others disperse it directly into the preparation of the membrane solution [27]. Darroudi [51] used an electrophoretic deposition (EPD) method for the deposition of graphene oxide (GO) nanosheets on the surface of SPE. Otherwise, El-Hanboushy et al. [50] took advantage of polypyrrole (PPy) films synthesized by electro-polymerization to form a uniform and adherent coating.

The most studied interface materials are carbon nanostructures (CNTs) in single or multiple forms and conductive polymers (CPs). Fig. 3 shows these different mechanisms in detail.

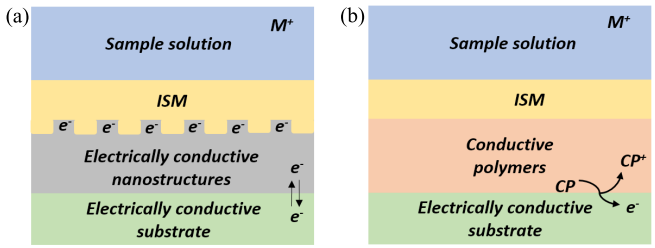

Fig. 3. (a) Scheme and working mechanism of ISEs with SCs based on conductive nanostructured (CNTs). (b) Scheme and working mechanism of ISEs with SCs based on CPs. M^+ represents the metal.

CNTs are based on the formation of an electrical double layer at the membrane/electrode interface for ion-electron transduction; thus, the trapping of ions on one side of the interface due to the role of the ISM, causes the accumulation of electrons and gaps. On the other side, this causes the generation of an asymmetric capacitor. In these systems, the interfacial potential is due to the amount of charge accumulated in the double layer. This leads to the accumulation of the potential difference. The large surface area facilitates adhesion, avoiding the risk of water absorption, while the high capacitance values reduce potential drift due to polarization effects caused by the small but different currents required for measurement. As interface materials, CPs are also highly exploited to date since they are capable of conducting both ions and electrons, and they can be exploited as effective ion-electron transducers using redox reactions. PPy, polyaniline (PANI), poly(3-octyl-thiophene) (POT), and poly(3,4-ethylenedioxythiophene) (PEDOT) are the most studied CPs in ASS-ISE today.

Rosenberg et al. [33] give a special case of nanotube use as the research group used carboxylated single-walled nanotubes. Elashery et al. [35] used CNT-modified graphite (CNTME) as the interface material.

Second, graphene is used, which has been used in different forms; for example, Li et al. [45] exploited GO film, and Yoon et al. [32] used reduced GO (rGO). Lia et al., who exploited 3-D self-assembled porous graphene aerogel (PGA) give another example. This method is useful because it can be conveniently and rapidly electrodeposited on the electrode surface [30].

Other interface elements that are printed are CPs, including poly(3,4-ethylenedioxythiophene) polystyrene sulfonate (PEDOT:PSS) [40], [46], [47], [49], [59], [62], POT [34], PANI [39], and PPy [50]. Some particular examples are given by the use of MWCNTs and polyaniline (f-MWCNTs/PANIs) used as ion-to-electron SC transducers [29], [53]. In addition, Ocaña et al. [42] functionalized poly (3,4-ethylenedioxythiophene) with methacrylate (Meth-PEDOT), and the Meth-PEDOT films contained either MWCNTs or carboxylated MWCNT (cMWCNT) were used as SCs.

Other interface structures are given by porous silicon nanostructures or are based on iron (Fe) nanohybrid loaded with 3-D honeycomb GO (GO-Fe)/zinc oxide (ZnO) nanoparticles [64].

As shown in Table II, graphene is the only sustainable material as it is biocompatible and biodegradable, so it can also be used inside the human body as it is tolerated and nontoxic; it is also a material that does not pollute in soil, water, and air. In fact, the idea of Elashery et al. [35] in using CNTME was excellent and innovative as they wanted to keep the concept green, and in addition to that they increased the efficiency of the interface material. In contrast to this, CPs such as PANI, PPy, PEDOT:PSS, and POT are not sustainable over time, so they tend to release toxicity into the surrounding environment in spite of their high conductivity. This also implies less use within the human body. Otherwise,

TABLE II
DIFFERENT TYPES OF INTERFACE MATERIALS WITH AN EVALUATION OF GREEN MATERIAL, DEPOSITION METHOD, AND DRYING TECHNIQUE. DC: DROP CASTING; EPD: ELECTROPHORETIC DEPOSITION; ED: ELECTROCHEMICALLY DEPOSITED; IJP: INKJET PRINTING; SP: SCREEN-PRINTING; CPEP: CONSTANT-POTENTIAL ELECTRO-POLYMERIZATION; EPG: ELECTRO-POLYMERIZED GALVANOSTATISTICALLY; DDMS: DIRECTLY DISPERSED IN MEMBRANE SOLUTION

Interface material	Deposition Method	Drying technique	Ref
CNTME	DC	Air drying	[35]
CNTs	DC	Air drying (3 min)	[25]
			[36]
		Drying at RT	[26]
		Air drying (5 min)	[37]
		Air drying	[31]
			[38]
			[56]
		2 h in a vacuum oven at 40°C	[43]
	ED	Air drying	[48]
	SP	N.A.	[28]
		10 min at 70 °C	[33]
		30 min at 50°C	[41]
			[55]
			[57]
Graphene	DDMS	Air drying	[27]
	DC	dried at 80 °C under vacuum for overnight	[32]
		Overnight evaporation RT	[44]
		Air drying	[54]
	EPD	2 h evaporation RT	[51]
	ED	immersion in deionized water and freeze-drying	[30]
		immersed in deionized water for 1 h removing residual GO absorbed on electrodes and dried	[45]
	IJP	Heat at 650 °C	[58]
Meth-PEDOT + MWCNT or cMWCNT	DC	Heated at 50°C	[42]
MWCNTs/PANI	SP	150°C	[29]
	DC	2 h evaporation RT	[53]
PANI	DC	Air drying	[39]
PEDOT and POT	CPEP (PEDOT) and DC (POT)	N.A.	[34]
PEDOT:PSS	DC	Air drying	[40]
			[49]
	ED	Dried in the moister buster cabinet	[46]
		N.A.	[47]
		N_2 drying	[62]
	IJP	Heated at 60 °C	[59]
PPy	EPG	Overnight evaporation RT	[50]

the characteristics of CNTs are special in that their conductive properties change depending on the geometry they possess.

C. Ion-Selective Membranes

In spite of the common mechanism among all the ISMs, which is to bind selectively ions, several different composition and fabrication methods can be found in the literature, both referring to the plasticizers and the selective elements employed. The plasticizer polymer most commonly used is polyvinyl chloride (PVC), which can, however, be found combined with different strategies for selective recognition. It has been observed that the thickness and hardness of the electrode membrane depend on the amount of PVC used. When more PVC is used, the membrane becomes stiff, too dense, and resistive. The result is a longer response time for potential measurement. Lower PVC content, however, makes the membrane too thin, resulting in poor mechanical strength, very rapid swelling in solution, and easy breakage. Increasing the amount of PVC will increase the thickness of the membrane electrode but sacrifice the elasticity of the membrane sheet [63].

Ali et al. exploited a macrocyclic membrane based on Schiff 2,6-pyridine dicarbometrine-triethylene tetramine (PDCTETA), an ionophore and ligand used to stabilize PVC against photodegradation by UV radiation, but also to improve polymethylmethacrylate from degradation and to prevent photodegradation of polystyrene. An idea that may be useful in improving the performance of the sensor and especially the membrane itself [55]. This material is poorly soluble in water and soluble in organic solvents; it is antifungal, antibacterial, antiinflammatory, antiviral, and antipyretic. Of interest are the properties of polyurethane [42] and acrylate [33] in general because they are recyclable and sustainable polymers.

One effective solution employed by several works is the combination of PVC with specific ionophores, molecules that can bind a single target ion of interest [25], [26], [29], [30], [31], [32], [34], [39], [41], [43], [44], [46], [47], [50], [51], [52], [54], [56], [57], [58], [59], [65]. To maximize detection performance, it is recommended to have an ISM cocktail that generally includes 1%–2% ionophore, 60%–70% plasticizer, and 30%–40% high molecular weight PVC. Examples of detection of an ion within a molecule involve the sulfite ion in beverages [29] or a noxious substance, e.g., pholcodine, an opioid-derived drug [28], [66]. PVC has several properties, such as strength, maintaining stiffness, impact resistance, excellent dimensional stability, mechanical properties, and resistance to abrasion and aging, chemicals, and fungal and bacterial attack; it is a lightweight material, and it is not sustainable.

Another innovative solution found in more recent literature employs special polymers associated with PVC, called molecularly imprinted polymers (MIPs) or nano imprinted polymers (NIPs), which are highly selective for the target ion, are used instead of the ionophore [27], [28], [36], [37], [38], [45], [49], [53]. These two types of membranes have mainly carbon atoms (not sustainable) and are stable at high temperatures (Fig. 4). In particular, an example of binding between the ionophore and the potassium ion is shown in Fig. 4(a). It can be seen

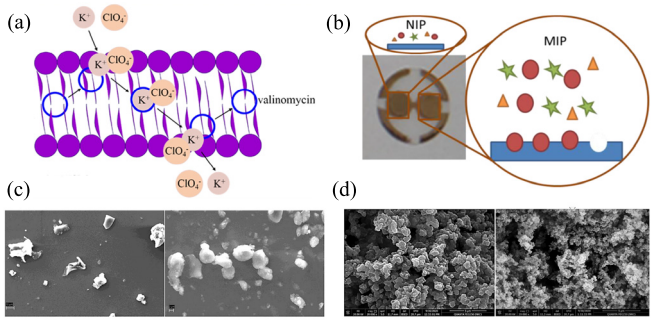

Fig. 4. Summary of the kind of membrane exploited to realize selective detection of ions in ASS-ISEs. SEM images reproduced from: showing (a) valinomycin incorporated into a biomimetic lipid membrane tethered to the surface of a gold electrode [70], (b) comparison between MIP and NIP beads [71], (c) comparison between SEM images for the surfaces of MWCNT-coated electrodes and PVC membrane (left) without ionophore and (right) with ionophore [72], (d) comparison between SEM images of (left) MIP and (right) NIP beads [28]. All the figures are from open-access articles under a Creative Commons License.

that the ionophore for the potassium ion is valinomycin [32], [33], [58], [59], a cyclic peptide used for detection/binding to this ion. This peptide can selectively transport alkali metal ions across biological and synthetic membranes. In fact, it can be seen from Fig. 4 that a biomimetic lipid membrane is used, which tends to mimic the cell membrane containing a large amount of lipids. Apart from this detail, it would be interesting to be able to print/develop biodegradable and environmentally sustainable membranes, including PVC, with all-natural materials, such as lipids, polysaccharides, or proteins.

The team of Ashmawy et al. [40] used selective materials in the sensing membrane, such as acetylcholine tetraphenylborate (ACh/TPB/PEDOT/PSS-ISE) (sensor I) and triacetyl-β-cyclodextrin (β-CD/PEDOT/PSS-ISE) (sensor II). Other groups, however, did not consider PVC as the polymer for the sensing membrane, but polyurethane-acrylate (PUA) [42]. The properties of this material are special, in that it does not age, does not discolor, it is temperature and moisture resistant, an inert material, does not rot, and is not penetrated by water, and it is sustainable (recyclable).

An additional example that does not take advantage of the PVC membrane is that of Rosenberg et al. [33] who used a plastic membrane for WE based on ionophores and a UV-curable polymer [Hexane-1,6 Diol DiAcrylate (HDDA)]. The latter material described instead has good chemical resistance and thermal and electrical properties and is sustainable (biocompatible). An alternative was the proposal of Zuliani et al. [62] in that they used ionogels based on bis(trifluoromethanesulfonyl)imide [NTf2] as a new salt-bridge material for REs. So, a capping membrane was used to prepare disposable SC ionogel REs (SCI-RE) [62]. Finally, Queirós et al. [48] used a sensing membrane as a sensing element, which is a plastic antibody designed by surface imprinting with carefully selected monomers to ensure a specific response.

Regarding fabrication techniques, drop-casting is still the most adopted [25], [26], [27], [28], [29], [30], [31], [32], [33], [34], [35], [36], [37], [38], [39], [40], [42], [44], [45], [46], [47], [48], [49], [50], [52], [53], [54], [56], [58], [62].

A limitation of this approach can be operator dependency; this does not appear to be a problem since in all the article-evaluated simple geometries with millimetric dimensions are used for the WEs, making manual drop-casting sufficiently precise for the functionalization; however, to improve the RP and the accuracy of electrodes covering with the membranes alternative techniques are starting to be investigated, including direct screen printing [41], [43], [55], [57] or inkjet printing [59] of the membrane alone or mixed with the ink for electrodes or interface layer. Direct printing of ISM represents a really promising approach to be better investigated in future works, in particular, exploiting noncontact techniques (e.g., inkjet printing (IJP), aerosol jet printing) to reduce material waste and optimize geometry thickness and resolution.

A wide variety of choices can be observed in terms of preconditioning of the membranes. The suggested concentration to condition the electrodes is usually the lowest standard of the calibration, which means the lower limit of the linear range required, or anyway, a concentration not more than one or two decades higher [28], [53], [66]. Several examples in the literature can, however, be found where concentrations higher than the upper range of the linear range were exploited for conditioning, without providing any reasons or tests to show an improvement of sensitivity at those concentrations [25], [54]. Actually, in light of the guidelines given by the International Union of Pure and Applied Chemistry (IUPAC) report [67], conditioning the sensing membrane in concentrated primary ion solutions cannot be recommended and may be disadvantageous concerning the attainable detection limit. Despite these guidelines, the preconditioning process still represents a significant source of variability that can strongly influence the result of sensor characterization, as investigated by Maksymiuk et al. [68]; thus, despite the incorporation of primary ion, occurring during the pretreatment step is essential to ensure stable performances; it can induce variability often underestimated by subject literature. This includes the accumulation and release of species that can affect linear range and LOD. This explains why it is fundamental to report accurately any pretreatment and operation step together with sensor calibration, ensuring their RPR for any successive use. Another interesting solution investigated in the literature to reduce the variability related to preconditioning protocols is the direct loading of primary ion solution in the membrane cocktail [69].

V. Metrological Characteristics

In this section, the main metrological parameters useful to fully characterize printed ASS-ISEs performances are described and deepened. For each parameter, the definition and computational methods employed in the analyzed literature are provided, trying to highlight a possible uniform method according to the indication of IUPAC and metrology best practices; furthermore, the contribution that printing process parameters, postprocessing methods, and set-up assembling can have on each parameter is evaluated. For each parameter, particular emphasis is given to highlighting the potentiality that novel printing techniques can provide, even going beyond what is found in the selected articles.

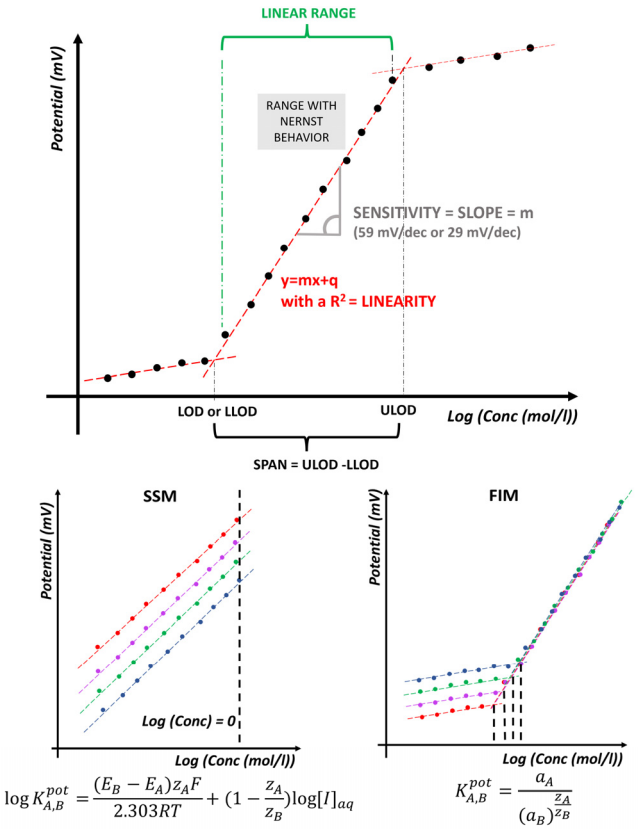

Fig. 5. Graphical example of how the main metrological characteristics of ISEs are computed. (a) Details sensitivity, LOD, span, and linearity. (b) Schematize how selectivity coefficients can be computed with the SSM performing separate calibration of different interferents and then taking the potentials corresponding to the logarithm of the concentration equal to zero for the equation shown. (c) Schematize how selectivity coefficients can be computed with the fixed interference method (FIM), performing different calibrations of the target analyte with a background of different interferents.

A. Sensitivity

The sensitivity in ASS-ISEs refers to the slope of the calibration curve, expressed as V/decade, obtained testing the response of the sensor in a range of concentrations where the sensor exhibits a Nernstian behavior corresponding to the working range of the sensor. A linear relationship can be obtained when the voltage is plotted against the logarithm in base 10 of the concentration of the target ion (Fig. 5) [as shown in (2)]. Together with linear range, it is one of the most relevant indicators of ISE performance and suitability for specific applications. As can be observed in (3), the theoretical slope should be equal to 59 mV/dec for monovalent ions and 29 mV/dec for divalent ions; thus, these represent the typical values to address when calibrating a new sensor. In experimental results, however, these values are not always attained, not only due to improper preconditioning (as explained in Section IV-C) but also due to several fabrication factors that can influence the transduction mechanism.

Focusing on printed ASS-ISEs, the main design parameters that can affect sensitivity are electrical or electrochemical properties of the printed interface layer and chemical composition of the membrane mix or ink in those cases in which it is

TABLE III
SENSITIVITY PARAMETER. GNPS: GRAPHENE NANOPARTICLES; NATPB: SODIUM TETRAPHENYLBORATE; PTA: PHOSPHOTUNGSTIC ACID; PMA: PHOSPHOMOLYBDIC ACID; RN: AMMONIUM REINECKATE; DOP: DIOCTYL PHTHALATE; o-NPOE: 2-NITROPHENYL OCTYL ETHER; β-CD OR TCP: TRIACETYL-β-CYCLODEXTRIN; MSPES: MODIFIED SCREEN-PRINTED ELECTRODES; DOS: DIOCTYLSEBACATE

Target Analyte	Sensitivity (mV/dec)	Ref
ACh	56.4 ± 0.6 (ACh/TPB/PEDOT/PSS-ISE) 55.3 ± 1.1 (β-CD/TPB/PEDOT/PSS-ISE)	[40]
AML; VAL	AML: 55.416; VAL: -29.829	[50]
Bacterial toxins	-62	[48]
Ca^{2+}	29.3 ± 1.0	[42]
Caffeine	51.2 ± 0.9	[27]
$Ce_{(III)}$	19.63 ± 0.51 (SPE)	[55]
CHX	28.8 ± 0.2	[54]
CLM	-55.42	[44]
COD	58.18 ± 0.81 (MWCNTs) 62.93 ± 0.98 (GNPs-SPE)	[56]
$Cr_{(III)}$	−29.7 ± 0.5 (paper) and −28.6 ± 0.3 (ceramic)	[39]
Cu^{2+}	28.7 ± 1.5	[30]
DCV-TPB	31.0 ± 1	[43]
DQ	28.2 ± 0.7	[49]
$Fe_{(III)}$	20.4 ± 0.30 (MSPEs-TCP) 19.6 ± 0.28 (MSPEs-DOS)	[41]
FLV	55.2 ± 0.4 (MIP-DOP)	[36]
FLX	56.2 ± 0.8 56.3 ± 1.7 64.4 ± 0.2	[25]
	58.9 ± 0.2 (MIP-TPB-o-NPOE)	[37]
H^+	-55.7 ± 0.5	[46]
K^+	53.34	[32]
	53.29 ± 2.78	[33]
	57.2	[58]
Na^+; K^+	56.4 ± 2.2 (Na^+; POT) 54.3 ± 1.5 (K^+; POT)	[34]
	Na^+: 62.5 ± 2.1; K^+: 62.9 ± 1.1	[59]
Na^+; NH_4^+	60.0 ± 4.0 (Na^+) 56.2 ± 2.3 (NH_4^+)	[31]
2-naphthoic acid	-59.0	[45]
Na^+	55.5 ± 4.9	[47]
	56.7	[62]
NaDC	-60.1 ± 0.9	[38]
NAL	60.3 ± 1.2	[53]
Ni^{2+}	30.4	[51]
$Pb_{(II)}$	28.98 ± 0.92 (SPE) 30.28 ± 0.70 (MWCNT-SPE)	[57]
PHO	31.6 ± 0.5	[28]
SO_3^{2-}	-29,8 ± 0.4 (MWCNTs); -26.5±0.6 (PANI); -28.8±0.7 (bare C)	[29]
TBAB	60.71±1.94 (NaTPB-SPE) 59.75±0.38 (PTA-SPE) 59.73±0.76 (PMA-SPE) 59.90±0.51 (RN-SPE)	[35]
TOLP	55.949	[52]

directly screen printed [41], [43], [55] or inkjet printed [59]. Regarding the interface layer, it can be appreciated from Table III that the sensitivity nearest to the theoretical value can be obtained only by exploiting nanostructures, in particular MWCNTs embedded in a polymeric matrix [52], or CPs, as in particular PEDOT:PSS alone [37] or in combination with other polymers [56].

B. Limit of Detection

The limit of detection, often referred to as LOD, represents one of the most adopted quantities to characterize the performances of ASS-ISEs and compare outputs among different sensors and solutions. LOD expresses the lowest quantity of ions that can be distinguished from the absence of that substance (a blank value) with a stated confidence level (generally 99%). The calculation of LOD in ASS-ISE characterization is different from the standard method commonly exploited for biochemical assays, relying on the three-sigma rule [73]. The recommended method by IUPAC [67] for determining LOD is by finding the point of intersection of the extrapolated lines of the Nernstian (high concentration) and nonresponsive (low concentration) segments of the calibration curve, where the Nernstian range corresponds to the range of concentration in which the sensor responds to Nernst equation. This specific LOD can be further referred to as lower LOD (LLOD). This is a definition used in several works to distinguish it from the upper LOD (ULOD), which defines the maximum concentration of ions of the linear range and starts decreasing the sensitivity [74]. The LLOD and the ULOD can also be seen as the limits of the so-called "span." The span of an ISE has been defined by IUPAC as the potential difference between the upper and lower detection limits of the electrode [75]. In spite of both ULOD and span being defined by IUPAC, they can rarely be found in the characterization of ASS-ISEs. Often, ULOD is not evaluated because the range of concentration tested is below the upper limit of the Nernstian range, being the interest toward lower concentration. Further, span, as defined by IUPAC in the literature related to ISEs is rarely used but is often replaced with linear span, which is, however, not superimposable (see Section V-C). A graphical example of how LLOD, ULOD, span, and linear range are computed is reported in Fig. 5.

Among the work analyzed on printed ASS-ISE (Table IV), excellent LOD has been reported in [45], where the best LOD so far, 6.9×10^{-11} M is obtained for 2-naphthoic acid. Other very interesting LODs are given by Queirós et al. [48] with 6.92×10^{-10} and Ali and Mohamed [55] with 5.24×10^{-9}.

The most important factors that can mainly influence the LOD and that could be optimized to improve its value are the velocity and continuity with which the ions contained in the sample are diffusing on the selective membrane. An interesting advantage that the printed process could bring to improve the uniform diffusion of ions refers to the possibility of integrating electrodes with customized microfluidics. Thanks to additive manufacturing techniques, it is possible either to directly fabricate printed microfluidic channels on top of printed electrodes [76] or to directly print electrodes on top of nonconventional porous materials enabling liquid flow (e.g., cellulose) [77] and then define proper path thanks to insulating materials (e.g., wax) [78]. In recent years, the detection limits of printed ISEs have been improved by several orders of magnitude [79], achieving nM and pM detection limits, exploiting mainly nanostructures-based modification of electrodes and interface layers, similar to what has been highlighted for sensitivity. MWCNTs and SWCNTs appear to be the most employed ones to enhance LOD, so they are not only used as an interface material but also incorporated into the electrode, helping to reduce the LOD to levels below 10^{-11} M [48]. This can be explained not only by thinking about the intrinsic electronic properties of CNTs but also by the combination of those properties with the finest control

TABLE IV
LOD PARAMETER

Target Analyte	LOD (M)	Ref
ACh	2.0×10^{-7} (ACh/TPB/PEDOT/PSS-ISE); 3.2×10^{-7} (β-CD/TPB/PEDOT/PSS-ISE)	[40]
AML; VAL	AML: 2.5×10^{-6}; VAL: 6.3×10^{-6}	[50]
Bacterial toxins	$6.92\times10^{-10}\pm2.8\times10^{-11}$	[48]
Ca^{2+}	$(3.4\pm3.1)\times10^{-6}$	[42]
Caffeine	3.0×10^{-6}	[27]
$Ce_{(III)}$	5.24×10^{-9}	[55]
CHX	4.76×10^{-7}	[54]
CLM	1×10^{-5}	[44]
COD	3.45×10^{-6} (MWCNTs); 2.20×10^{-6} (GNPs-SPE)	[56]
$Cr_{(III)}$	2.5×10^{-5} (paper); 2.4×10^{-6} (ceramic)	[39]
Cu^{2+}	$10^{-6.5}$	[30]
DCV-TPB	8.5×10^{-7}	[43]
DQ	0.026 µg/mL	[49]
$Fe_{(III)}$	2.6×10^{-7} (MSPEs)	[41]
FLV	4.7×10^{-6} (MIP-DOP);	[36]
FLX	5.2×10^{-6} 4.7×10^{-6} 2.0×10^{-7}	[25]
	2.1×10^{-6} (MIP-TPB-o-NPOE)	[37]
$Pb_{(II)}$	1.0×10^{-7} (SPE) 4.6×10^{-8}; (MWCNT-SPE)	[57]
K^+	−4.24 log[K+], 0.06 mM	[32]
	6.22 ± 0.48	[33]
	$10^{-5.2}$	[58]
Na^+; K^+	Na^+: 3.2×10^{-5} ; K^+: 1.01×10^{-4}	[59]
2-naphthoic acid	6.9×10^{-11}	[45]
NAL	4.5×10^{-7}	[53]
Ni^{2+}	2.0×10^{-7}	[51]
ODV	2.0×10^{-6}	[26]
PHO	2.5×10^{-7}	[28]
SO_3^{2-}	1.1×10^{-6} (MWCNTs); 1.5×10^{-6} (PANI); 2.7×10^{-6} (bare C)	[29]
TOLP	2×10^{-5}	[52]

TABLE V
LINEARITY AND CORRELATION (R OR r) PARAMETERS; IPHORE: IONOPHORE

Target Analyte	Linearity (M)	Correlation (R^2 or r)	Ref
ACh	1.0×10^{-6}–1×10^{-3} (ACh/TPB/PEDOT/PSS-ISE) 2.0×10^{-6}–1.0×10^{-3} (β-CD/TPB/PEDOT/PSS-ISE);	R^2: 0.999 (ACh/TPB/PEDOT/PSS-ISE) 0.998 (β-CD/TPB/PEDOT/PSS-ISE)	[40]
AML; VAL	AML: 3.0×10^{-6} to 1.0×10^{-3} VAL: 1.0×10^{-5} to 1.0×10^{-3}	N.A.	[50]
Bacterial toxins	1.32×10^{-9} to 7.75×10^{-10}	N.A.	[48]
Ca^{2+}	10^{-7}–10^{-2}	N.A.	[42]
Caffeine	4.5×10^{-6}–1.0×10^{-3}	R^2: 0.997	[27]
$Ce_{(III)}$	1×10^{-8} to 1×10^{-1} (SPE)	r: 0.999 (SPE)	[55]
CHX	10^{-6} to 10^{-3}	r: 0.9998	[54]
CLM	1×10^{-2} to $1\times10^{-5.3}$	R^2: 0.9936	[44]
COD	4.88×10^{-6}–1×10^{-2} (MWCNTs) 2.44×10^{-6}–1×10^{-2} (GNPs-SPE)	r: 0.996 (MWCNTs) 0.999 (GNPs-SPE)	[56]
$Cr_{(III)}$	7.5×10^{-3}–5.0×10^{-5} (paper) 7.5×10^{-3}–1.0×10^{-5} (ceramic)	R^2: 0.9977 (paper) 0.9996 (ceramic)	[39]
Cu^{2+}	10^{-6}–10^{-3}	R^2: 0.992	[30]
DCV-TPB	N.A.	$R^2 = 0.9999$	[43]
DQ	10^{-6}–10^{-2}	R^2: 0.999	[49]
$Fe_{(III)}$	N.A.	r: 0.999(TCP-MSPE); 0.997 (DOS-MSPE)	[41]
FLV	10^{-5}–10^{-3}	$R^2 = 0.999$	[36]
FLX	6.5×10^{-6} to 10^{-2} (Iphore I); 5.6×10^{-6} to 10^{-2} (Iphore II); 2.0×10^{-7} to 10^{-2} (Iphore III)	N.A.	[25]
	1.0×10^{-2}–5.5×10^{-6} (MIP-TPB-o-NPOE);	R^2: 0.999 (MIP-TPB-o-NPOE);	[37]
H^+	N.A.	$R^2 > 0.998$	[46]
K^+	2.5×10^{-1}–6×10^{-5} (250–0.06 mM)	N.A.	[32]
	10^{-5}–10^{-2}	N.A.	[58]
Na^+; K^+	log(a) = -4.0 to -1.0 (Na^+); log(a) = -4.0 to -0.5 (K^+)	N.A.	[34]
	10^{-4} to 1 M	N.A.	[59]
Na^+	10^{-5} to 10^{-1}	$R^2 > 0.98$	[47]
NaDC	N.A.	R^2: 0.999	[38]
NAL	2.4×10^{-7} to 3.3×10^{-3}	R^2: 0.999	[53]
Ni^{2+}	1.0×10^{-4} to 3.0×10^{-7}	N.A.	[51]
ODV	7×10^{-5} to 1×10^{-3}	R^2: 0.999	[26]
$Pb_{(II)}$	1.0×10^{-7} – 1.0×10^{-1} (SPE) 4.6×10^{-8} -1.0×10^{-1} (MWCNT-SPE)	N.A.	[57]
PHO	5.5×10^{-6}	R^2: 0.998	[28]
SO_3^{2-}	2.0×10^{-6} to 2.3×10^{-3} (MWCNTs) 5.0×10^{-6} to 2.3×10^{-3} (PANI);	R^2: 0.998 (MWCNTs); 0.999 (PANI) 0.999 (bare C)	[29]
TBAB	1.0×10^{-5} to 1.0×10^{-2} M	R^2: 0.999	[35]
TOLP	5×10^{-5} to 1×10^{-2}	R^2: 0.9998	[52]

in their deposition provided by the high-resolution printing technique. This can reduce the variability in the geometry patterning and the amount of CNT deposition, thus reducing the background noise that strongly affects LOD [21].

C. Linear Working Interval Range and Linearity

The main parameters employed to characterize the range of concentrations, where the ISE has a Nernstian response, include linear working range and correlation coefficient. Together with LOD and sensitivity, these parameters can be obtained from the calibration curve. In detail, the linear working range or linear range or linearity range represents the range of concentrations in which the calibration curve can be considered linear, which means that the sensitivity is constant since the intensity of the signal obtained is directly proportional to the concentration of the species producing the signal [80] (see Fig. 5 for the differences with span and concentration range).

The correlation coefficient (commonly defined as R^2) provides a quantification of the linearity of the calibration curve. Its value is included in the range between 0 (completely uncorrelated) and 1 (perfectly correlated), and it defines the goodness of the linear regression, guiding the definition of the most suitable linear working range. In some works, linearity evaluation is extended, and it includes other quantitative parameters related to the regression line, such as the intercept, the slope, and other specific metrological characteristics such as precision, RP, and accuracy [44]. These additional characteristics are, in most cases, considered separately, since they are not strictly related to the linear behavior of the sensor.

In terms of numerical parameters observed in the works analyzed (Table V), the best performances obtained in terms of linearity range, are the eighth order of magnitude (from 10^{-8} to 10^{-1}) covered by the linear range of SPE sensors toward $Ce_{(III)}$ proposed in [55] and by the MWCNTs-SPE for $Pb_{(II)}$ proposed in [57].

The main factors that can affect the linearity are related to physical parameters of the solution tested (e.g., temperature

and pH), the target ions diffusion at the sample-membrane interface, and the interference of nontarget analytes. The possibility provided by printing techniques to integrate easily more than one electrode in the same chip represents a powerful tool for obtaining multisensing platforms. This can be exploited to perform single or multitarget ion detection with simultaneous monitoring of side parameters such as pH, temperature, or sample volume quantification [81], [82].

The design of the sensor can, furthermore, have an impact on linearity in particular in terms of a stable interaction between the different layers that constitute the electrode (electrode, interlayer, and selective membrane), stable and selective membrane, and further stable RE; thus, both sensitivity and linearity suffer from what could have been achieved with a perfectly stable RE potential. The deviation from the ideal response might increase both with time and analyte concentration [83]. Interesting strategies to improve the linearity dealing with printed ASS-ISEs refer to both the fabrication of WE and RE. Regarding WE, a solution to improve the stability of the interaction between the different layers is to embed materials with different roles in a single ink. Interesting examples can be found integrating nanostructures of the interlayer in the electrode ink [41], integrating the membrane directly with the interlayer solution [27], and customizing a single ink acting as an electrode, interlayer, and selective membrane [55], to improving the interaction between each layer. Regarding RE, the main strategy refers to the printing of a PVB membrane together with the ink for RE [31].

D. Selectivity

Selectivity represents the ability of ISEs to correlate changes to a specific ion, reducing the cross-sensitivity, and thus, detecting a given ion in a sample containing a mixture of other analytes and contaminants. This metrological parameter represents one of the most discussed, criticized, misinterpreted, and misused terms of the IUPAC recommendations [67]. As shown in Table VI, although most articles report the quantitative calculation of selectivity coefficients, this parameter was not evaluated or was evaluated only qualitatively [31], [46], [47], [62], [64], [65], [84]. These coefficients, usually defined as $K^{\text{pot}}_{\text{A,B}}$, quantify the selectivity for the primary ion A concerning an interfering ion B. A small selectivity coefficient implies a low level of interference, and thus, a good level of selectivity [85]. As defined by IUPAC, the selectivity coefficients compare in the Nikolsky-Eisenman equation (3), which can thus be exploited as a starting point to obtain each coefficient for each interfering analyte (4). Essential prerequisites are that both target and interfering ions exhibit a Nernstian response and the same charge

$$E = E_0 + \frac{RT}{zF} \ln\left[a_{\text{A}} + \sum_{\text{B}} K^{\text{pot}}_{\text{A,B}} (a_{\text{B}})^{\frac{z_{\text{A}}}{z_{\text{B}}}}\right] \quad (3)$$

$$\log K^{\text{pot}}_{\text{A,B}} = \frac{(E_{\text{B}} - E_{\text{A}}) z_{AF}}{2.303RT} + \left(1 - \frac{z_{\text{A}}}{z_{\text{A}}}\right) \log a_{\text{A}} \quad (4)$$

where E_0 is a constant, including the standard potential of the electrode; a_{A} and a_{B} are the activities of the target and interfering ions, respectively; z_{A} and z_{B} their valence; $K^{\text{pot}}_{\text{A,B}}$

TABLE VI

SELECTIVITY PARAMETER. TA: TARGET ANALYTE; IA: INTERFERING ANALYTE; HCT: HYDROCHLOROTHIAZIDE; SLS: SODIUM LAURYL SULFATE; DS: DICLOFENAC SODIUM; GLUT: DL GLUTAMATE; $C_8H_{17}NO_2$: PREGABALIN; $C_{16}H_{26}ClNO_2$: TRAMADOL HCl; R: ARGININE; $C_{16}H_{16}F_3NO$: NORFLUOXETINA; $C_{17}H_{27}NO_2$: VENLAFAXINE; $C_{10}H_{15}NO$: EPHEDRINE; $C_{17}H_{19}NO_3$: MORPHINE; IBU: IBUPROFEN; $C_{22}H_{30}N_6O_4S$: SILDENAFIL; PQ: PARAQUAT; DX: DEXTROSE; GLU: GLUCOSE; IPHORE: IONOPHORE

TA	Best Selectivity (logK or K)	IA	Worst Selectivity (logK or K)	IA	Ref
ACh	logK -7.3	Mg^{2+}	logK -1.1	$C_{17}H_{19}NO_3$	[40]
AML VAL	AML: logK -3.89 VAL: logK -3.18	$ZnSO_4$(AML) $MgSO_4$(VAL)	AML: logK -2.08 VAL: logK -1.84	HCT	[50]
Ca^{2+}	logK -3.8	Mg^{2+}	logK -3.1	Li^+	[42]
$Ce_{(III)}$	logK -6.11	Na^+	logK -2.23	Y^{3+}	[55]
CHX	K 2.69×10^{-3}	Pb^{2+}	K 1.36×10^{-6}	SLS	[54]
Caffeine	logK -5.8	Na^+	logK -2.4	$C_{10}H_{15}NO$	[27]
CLM	logK -4.09	$MgSO_4$	logK -2.84	NaCl	[44]
COD	K: 2.00×10^{-3} (MWCNTs) K: 4.79×10^{-3} (GNPs)	DX (MWCNTs); Glu (GNPs)	K: 8.32×10^{-3} (MWCNTs) K:9.95×10^{-3} (GNPs)	IBU (MWCNTs); KCl (GNP)	[56]
$Cr_{(III)}$	Paper logK -5.8; ceramic logK -5.5	ClO_4^-	Paper logK 0.7; ceramic logK -0.2	I^-	[39]
Cu^{2+}	logK -3.7	Cd^{2+}	logK -1	Pb^{2+}	[30]
DCV-TPB	logK -4.24	Ca^{2+}	logK -3.04	NH_4^+	[43]
DQ	logK -6.7		logK -3.5	PQ	[49]
FLV	with MWCNT: logK -3.85; no MWCNT: logK -4.22	R	with MWCNT: logK -2.94; no MWCNT: logK -3.01	$C_{17}H_{27}NO_2$	[36]
FLX	logK -5.8 (Iphore I) logK -4.9 (Iphore II) logK -5.6 (Iphore III)	R(Iphore I&III); Ba^{2+} (Iphore II):	logK -1.0 (Iphore I) logK -0.7 (Iphore II) logK -1.5 (Iphore III)	$C_{16}H_{16}F_3NO$	[25]
	- logK 7.1 (DOP) - logK 6.1 (o-NPOE) - logK 7.1 (o-DOS)	R	- logK 3.2 (DOP) - logK 2.8 (o-NPOE) - logK 3.5 (o-DOS)	$C_{22}H_{30}N_6O_4S$	[37]
K^+	logK -4.7	Ca^{2+}	logK -1.7	NH_4^+	[33]
	logK -7.98	Ca^{2+}	logK -2.99	NH_4^+	[32]
	log K -3.90;	Mg^{2+}	log K -0.12;	Na^+	[58]
Na^+;K^+	Na^+: logK -2.85 K^+: logK -3.11	Ca^{2+} (Na^+); Mg^{2+} (K^+)	Na^+: logK -1.86 K^+: logK -2.16	K^+ (Na^+); Na^+ (K^+)	[59]
NaDC	logK -3.6	Creatinine	logK −1.7	$C_2O_4^{2-}$	[38]
NAL	logK -8.5	$C_8H_{17}NO_2$	logK -4.5	$C_{16}H_{26}ClNO_2$	[53]
Ni^{2+}	K 1.1×10^{-4}	Mg^{2+}	K 4.1×10^{-3}	Cu^{2+}	[51]
ODV	logK -5.8	R	logK -2.6	$C_{17}H_{27}NO_2$	[26]
$Pb_{(II)}$	logK -6.20 (SPE, SSM) logK -6.21 (MWCNT-SPE, SSM)	K^+	logK -1.01 (SPE, SSM) logK -1.05 (MWCNT-SPE, SSM)	Fe^{3+}	[57]
PHO	logK -5.5	Ca^{2+}	logK -1.5	$C_{17}H_{19}NO_3$	[28]
SO_3^{2-}	logK -6.3 (MWCNTs) logK -6.1(PANI) logK -6.2 (bare C)	PO_4^{3-}	logK -4.2 (MWCNTs) logK -4.5 (PANI) logK -4.1(bare C)	NO_3^-	[29]
TBAB	1.26×10^{-4} (NaTPB) 7.64×10^{-6} (PTA) 5.62×10^{-5} (PMA) 1.12×10^{-6} (RN)	Cr^{3+} (NaTPB); Pb^{2+} (other)	6.31×10^{-4} (NaTPB) 6.56×10^{-2} (PTA) 1.04×10^{-2} (PMA) 1.31×10^{-2} (RN)	Pb^{3+}; (NaTPB); Al^{3+} (other)	[35]
TOLP	logK -3.45	DS	logK -2.41	Glut	[52]

the potentiometric selectivity coefficient of the target ion A against the interfering ion B.

In the reviewed articles, two main approaches, in agreement with IUPAC recommendation, are followed to compute selectivity coefficients, as graphically reported in Fig. 5. The first one is the separate solution method (SSM) [30], [32], [35], [40], [44], [50], [51], [53], [54], [56], [59], [86], based on the use of two different solutions for the measurements: one containing only target ions A at a certain concentration and the second with only interfering ions B at the same concentration; in some works this method is presented as a modified SSM (MSSM) [26], [27], [28], [29], [36], [37], [38], [39], [66], [87], with the only difference that the log Conc versus E relations of an ISE for the primary and interfering ions are obtained independently, and then, the activities that correspond to the same electrode potential value are used to determine the K. The second method is called the fixed interferent method [25], [33], [34], [43], [55], or sometimes referred to as the mixed solution method [42]. It is based on the use of solutions containing interfering ions at a constant concentration and varying concentration of the target ion. In some cases, these primary methods are combined with other strategies, such as matched potential method (MPM) [41], [55], [57]. In detail, knowing the activity of the target ion, the associated variations in potential (E/mV) were measured. Following that, an interfering ion solution was added to the reference target solution until the same potential change (E/mV) was seen. Technically, MPM is the only method enabling the evaluation of neutral species, accounting for a more realistic approach and applying it to sensors that do not show Nernstian responses [48]. Another method proposed by a few works [45], [58] is Bakker's method, which suggested eliminating the influence of the inherent sensitivity limit on the ISE response toward interfering ions.

In terms of numerical parameters observed in the works analyzed proposing printed ASS-ISEs (Table VI), coefficient values appeared widely distributed depending on the kind of interfering agents tested, with most of the selectivity coefficients in a range between 10^{-3} and 10^{-6}. Only a few articles show results better than this range. The best selectivity obtained employing a traditional PVC-based membrane with ionophores were values of the coefficients K^{pot} lower than 10^{-7} in [32] and [40], combined either with reduced graphene or with PEDOT:PSS interlayer, while the lowest coefficient value of $10^{-8.5}$ was obtained in [53] employing MIP/NIP-PVC membrane combined with a MWCNTs/PANI interlayer.

The main design specification that can affect selectivity is the protocol of preparation and deposition of the selective membrane on top of the WE. In particular, selectivity is strongly related to the ionophores mixed in the chemical solution to realize a plastic membrane. The stability of the composition of the membrane during all the phases of its preparation (mixing, deposition, drying, storage) needs to be carefully preserved to avoid issues in terms of selectivity. This is particularly true for those, up to now limited, cases in which the membrane is deposited on top of the electrodes using printing methods [41], [43], [55], [57], [59], [68]. In these cases, it is particularly important during the printing process to be able to control the physical parameters (e.g., temperature, pressure, humidity) that the ink is undergoing during the process of droplets or aerosol formation, but also membrane drying on top of the printer plate. The advantages offered by printing processes in terms of geometrical control and thickness control, even on 3-D surfaces, can also help to better optimize the area covered by the selective membrane not only on flat electrodes but also on unconventional substrates, thus maintaining the same selectivity with reduced waste and cost of materials [88]. Further, the combination of powerful printing techniques enabling high-resolution patterns with specific postprocessing treatments could contribute to exploiting innovation concerning the examples shown, fabricating novel membranes based on oriented channels with customized dimensions [89].

E. Stability

The stability of ASS-ISEs represents the degree of susceptibility to environmental disturbances and other factors that could take place in and/or around the sensing system. The output of an unstable biosensor typically presents a drift that affects the quality of the measurement information. Stability represents an important parameter evaluated both during short-term measurements (short-term stability, typically evaluated in time windows of minutes or hours) but also when the sensor is applied in applications envisioning long-term continuous monitoring of the measurand (long-term stability, typically evaluated in time windows of days, weeks or months). Even in the short term, electrode potential stability is a major challenge for ASS-ISEs [11], with the formation of a water layer in the ion-to-electron transducer being the main cause of electrode potential instability. The water layer test commonly represents the main method for the characterization of potential stability due to the formation of an aqueous layer. This is based on the measurements of the potential during successive exposures of the sensor to concentrated solutions (e.g., 0.1 M) of target and interfering ions for several hours. Even small ionic fluxes during ion exchanges can lead to large changes in the very thin water layer at the ISE/SC interface, leading to positive and negative drifts during exposure to the interfering and target ion, respectively [37], [42], [50], [59]. Long-term stability instead is evaluated during time frames of days or weeks, computing at discrete time points the value of the slope in mV/decade [55].

Stability is one of those metrological parameters that is not uniformly stated throughout the literature, as many researchers limit themselves to testing the stability of sensors only for 1 h [31], [52], while others go on to evaluate long-term stability, such as lasting six months [53] or about seven months [41], [55]. In addition, when sensor stability is evaluated over a long period, potential drift, understood as electrical potential over time, is also defined. Again, there is no uniformity in the description of metrology because there is great confusion in the given units of measurement, and there is no fixed international system. Based on this, many researchers persist in only providing potential drift as a stability value, with values ranging around 10 μV/s [32], [34], [38], [43], [46], [58] (Table VII).

TABLE VII
STABILITY PARAMETER

Target Analyte	Stability (weeks)	Ref
AML; VAL	9	[50]
Caffeine	1.43	[27]
CHX	1.43	[54]
CLM	4	[44]
$Cr_{(III)}$	7	[39]
DCV-TPB	70 mins	[43]
DQ	7	[49]
$Fe_{(III)}$	25	[41]
FLV	28.57	[36]
FLX	24	[25]
	2.14	[37]
NaDC	7	[38]
NAL	60 mins	[53]
Na^{+}	4 hours	[47]
Ni^{2+}	9	[51]
ODV	1.43	[26]
PHO	8.57	[28]

Regarding design choices, the selection of the electrically conductive substrate and the type and thickness of the interface layer plays an important role in stabilizing the potential of ASS-ISE when it encounters a solution for the first time. The beneficial effect of electrode nano-structuration or the deposition of polymers on potential stability is evident in both cases in terms of a reduction of the drift in the potential when the ISE is exposed to a fixed concentration [37], [50]. On the contrary, bare electrodes fabricated with non-nanostructured conductive materials or without any polymeric coating show a major potential instability, as evident from the graph slope in Fig. 6; furthermore, hydrophobic materials are being investigated as potentially useful to reduce the water layer formation, and thus, increase the stability [90]. Further, other aspects of the fabrication process that can improve the stability refer to the RE and include the deposition of an additional polymeric layer (most frequently PVB) to protect and stabilize the electrode to maximize its ability to maintain the reference potential constant. Finally, since the progressive degradation of membrane composition can lead to long-term instability, particular attention needs to be addressed to the storage conditions and maximizing the usage time of the overall sensor.

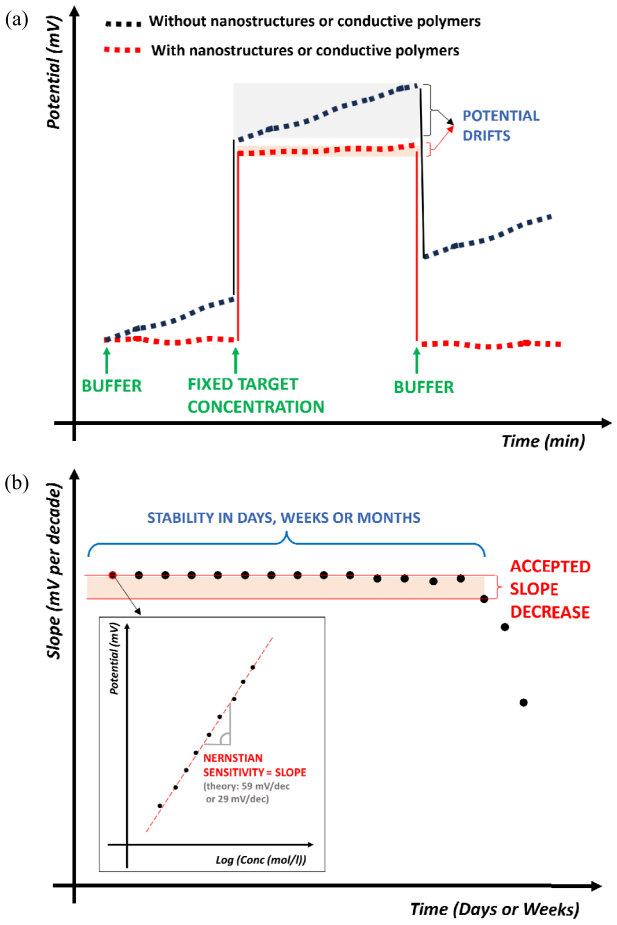

Fig. 6. Graphical example of how short- and long-term stability are usually computed to evaluate printed ASS-ISEs. (a) Scheme of the water layer test is typically performed to evaluate short-term stability. Potential drift is the quantitative parameter usually associated with this metric. (b) Scheme of how long-term stability is typically performed over days or weeks. Repeated calibrations are performed at discrete time points, the sensitivity computed and its value plotted against time. The time window in which the sensitivity (slope) decrease is maintained within a defined range is then computed.

F. Repeatability and Reproducibility

RP and RPR take into consideration the variability associated with the measurements, either intrinsically due to fabrication variability or extrinsically due to variability in the measurement protocol. The results are usually expressed as percent relative standard deviation (RSD) concerning average measurements. A lack of metrological rigor in distinguishing protocols and results for evaluating RP and RPR can be observed in evaluating the analyzed articles dealing with printed ASS-ISEs. In some cases, instead of referring explicitly to RP and/or RPR tests, researchers refer to precision but with a protocol description that also introduces the time as a variable, thus resembling the stability definition [56]. The difference between RP and RPR should only be in the setup exploited to perform replicated measurements to compute the RSD. RP is reported to be usually calculated by repeatedly measuring with the same sensor a solution containing the same concentration of target ion [25], [26], [44], [50], [54], or the same pattern of increasing and decreasing concentrations [32]. In most of the articles reporting RP tests, these are exploited to compute the instrument's precision; thus, this parameter is also often referred to as "intra-day precision" when the measurements are repeated at different times on the same day. Despite this second parameter has a relevant meaning, especially considering printed sensors that are degrading faster than the traditional bulk carbon paste electrodes, it would be more correct to define this as intraday stability or short-term stability; thus, time becomes an additional parameter for the traditional RP test, and it would be important to also associate the timing between the different measurements.

RPR, on the other hand, is calculated with measurements made with the same concentration but on different sets of sensors and different instruments at different times [25], [29], [49]. Even if in most of the articles where RPR is mentioned and is provided as percent RSD, in some of the articles [42],

TABLE VIII
RP AND RPR PARAMETERS; IPHORE: IONOPHORE

Target Analyte	RP (%)	RPR (%)	Ref
ACh	N.A.	1.7(ACh/TPB/PEDOT/PSS -ISE)	[40]
AML; VAL	AML:0.332; VAL:0.770	N.A.	[50]
Ca^{2+}	N.A.	11	[42]
$Ce_{(III)}$	0.082 (SPE)	N.A.	[55]
CHX	0.575	N.A.	[54]
CLM	1.516	N.A.	[44]
COD	1.02 (MWCNTs); 1.12 (GNPs-SPE)	1.23 (MWCNTs) 0.87 (GNPs-SPE)	[56]
$Cr_{(III)}$	0.9 (paper) 1.2 (ceramic)	1.2 (paper) 0.8 (ceramic)	[39]
DQ	0.9	1.1	[49]
FLX	2.1 (Iphore I); 2.2 (Iphore II)	2.3	[25]
K^+	2.9 mV	N.A.	[32]
Na^+; K^+	N.A.	Na^+: 1.2; K^+: 0.64	[59]
ODV	1.1	N.A.	[26]
SO_3^{2-}	1.1(MWCNTs); 0.8 (PANI); 0.9 (bare C)	0.4 (MWCNTs) 0.8 (PANI)	[29]

TABLE IX
RESPONSE TIME PARAMETER

Target Analyte	Response Time (s)	Ref
ACh	< 10	[40]
AML; VAL	AML: 5; VAL: 10	[50]
Bacterial toxins	< 20	[48]
Ca^{2+}	120 (2 min)	[42]
Caffeine	< 5	[27]
$Ce_{(III)}$	6–8	[55]
CHX	15	[54]
CLM	10	[44]
COD	15 (MWCNTs) 10 (GNPs-SPE)	[56]
$Cr_{(III)}$	< 10	[39]
DCV-TPB	< 15	[43]
DQ		[49]
$Fe_{(III)}$	6 (TCP-MSPE); 8 (DOS-MSPE)	[41]
FLV	10–20	[36]
H^+	< 10	[46]
K^+	6	[32]
	10	[58]
Na^+; K^+	180	[59]
NAL	< 20	[53]
Ni^{2+}	20	[51]
ODV	< 8	[26]
$Pb_{(II)}$	9 (SPE); 7 (MWCNT-SPE)	[57]
SO_3^{2-}	< 5	[29]
TOLP	≤ 10	[52]

[59] authors refer to the RPR of the standard potential E_0 providing the average with a standard deviation of the E_0 extrapolated from the linear section of the calibration curve to concentration = 1 (i.e. log $[I] = 0$). Of course, although the RSD can be calculated from the average and standard deviation provided, this method appears difficult to compare with most of the RPR given as RSD. Consequently, after reviewing the different methods for computing RP and RPR, the most useful and rigorous method appears to be the one that takes into consideration the replicated measurements performed during the same period, leaving the time variable for consideration in the stability metrics.

Focusing on printed ISE, the most significant factors that can affect RP and RPR are the variability of the printing process, the functionalization protocol, and the setup. Novel high-resolution techniques could improve process variability through better control at the deposition stage. This could avoid large variabilities between the area of conductive traces and electrodes and also help in improving the RP of the deposition of nanostructures following specific patterns [1]. Further, the possibility to directly embed the sensor with customized microfluidics, either on paper or with polymeric channels [47], [59], can improve the way the ion solution is delivered to the sensor, thus reducing RP and RPR (Table VIII). Finally, the possibility of directly printing the membrane, avoiding operator-dependent manual deposition, can strongly reduce the variability of the transducing step [41], [43], [55], [57].

G. Response Time

The response time is a quantitative indicator of the time needed by the biosensor to provide an output that can be reliably correlated with the concentration of the analyte tested. It is usually computed thanks to a dynamic calibration, evaluating the time needed from the output to reach a fixed percentage of the maximum steady-state values. For traditional sensors, the response time is usually the time needed to go from 10% to 90% of the steady-state value, while for biosensor validation, high variability in the meaning of response time can be found. In particular, response time should be measured, in agreement with the indication of IUPAC [91], as the time required to obtain a stable signal when the sensor is undergoing a specific concentration spike, with a steady state value within 1 mV [27], [51]. It is commonly calculated by isolated assessments in the form of steps from low to high concentrations. Often, the same method is applied but with steps in the opposite direction to evaluate the response time in case of decreasing concentration and thus assess the reversibility of the system. An important recommendation given by IUPAC, not always followed by the articles analyzed, which could improve the possibility of comparing the data among different works, is to associate the definition of the response time with the specific experimental conditions the ASS-ISE is undergoing (i.e. the stirring rate, the composition of the solution, the history and preconditioning of the electrode, and the temperature), since these values could strongly affect response time.

The main aspects that can affect response time regard the integration of the ASS-ISEs within a suitable microfluidic system that should be able to continuously supply the sensing area with new samples to be analyzed [47]. For example, in [31], microfluidics combined with CNTs added to the sensing membrane has been highlighted as a key element to improve response time together with sensitivity. Further aspects to be addressed to improve the response time refer to the conductivity of the electrode and the performances of the transducing layer in terms of conductivity to avoid introducing delays. GO [27], [32], MWCNTs alone [55], [57] or mixed with polymers [29] are the most suitable materials to obtain the lowest response time (Table IX).

H. Accuracy, Precision, and Recovery Rate

Other relevant metrics employed in several articles to evaluate the performance of ASS-ISEs are accuracy, precision, and recovery rate. In spite of these representing very useful indicators of the performances of ASS-ISEs, they are often reported without rigor and uniform definitions.

Accuracy represents a crucial parameter since before any new sensor can be accepted, it should be correlated with the standard method routinely used in the laboratories. It is, in fact, defined as the maximum divergence from the actual most reliable "gold standard" in terms of assay output. It should be expressed as a percentage of the output from the validated ISEs concerning the output of traditionally accepted laboratory equipment [29]. In spite of most of the referenced articles appropriately using the term accuracy, in some of the works, this parameter appears to be mistakenly confused with precision. Differently from accuracy, precision is not considered in the comparison of the new sensor with a gold standard output, but it is defined as the maximum divergence between measured values obtained multiple times, provided that variability between measured items (if similar and not equal) is taken into account [41]. A measurement is more precise when it offers a smaller random error while not being related to the systematic error [44]. The main parameters that can affect accuracy and precision are measurement errors and random errors. Random errors of a set of replicate measurements form a distribution that can be summarized by its average, which is generally assumed to be zero, and its standard deviation.

Another parameter that, in some examples, is cumulatively indicated as an indicator of accuracy and precision is the recovery rate [26]; sometimes, it is also defined as mean recovery or recovery value [26], [27], [48], [52]. The recovery rate is calculated from spike and recovery tests where a known amount of analyte is added (spiked) into real samples (e.g., sweat, saliva, water, or soil samples). Then, the ASS-ISEs output is measured (recovery) and compared to an identical spike in the standard diluent. This is particularly useful to assess variability that can be introduced by real samples with respect to standard laboratory solutions.

TABLE X
FIELD OF APPLICATION OF ASS-ISES AND TARGET ANALYTES

Field of application	Target Analytes	Ref
Drugs and molecules monitoring	Fluoxetine (FLX)	[25]
		[37]
	Desvenlafaxine (ODV)	[26]
	Caffeine	[27]
	Pholcodine (PHO)	[28]
	Fluvoxamine (FLV)	[36]
	Daclatasvir-tetraphenyl borate (DCV-TPB): Hepatitis C Antiviral Drug	[43]
	Clomipramine (CLM) assay in spiked plasma	[44]
	Antihypertensive Drugs - cationic amlodipine (AML) and anionic valsartan (VAL) in binary and ternary mixtures with hydrochlorothiazide (HCT)	[50]
	tolperisone HCl (TOLP) + diclofenac sodium and paracetamol as co-formulated drugs	[52]
	nalbuphine (NAL) in pharmaceuticals and biological fluids	[53]
	Chlorhexidine Digluconate (CHX)	[54]
	codeine phosphate in the presence of ibuprofen in pharmaceutical and biological matrices (COD)	[56]
Ions detection in biofluids	Sodium, ammonium (Na^+, NH_4^+)	[31]
	Sodium, potassium (Na^+, K^+)	[34]
		[59]
	Sodium Deoxycholate (NaDC)	[38]
	Neurotransmitter and Acetylcholinesterase Detection in Human Serum (ACh)	[40]
	K^+	[58]
	Na^+	[47]
		[62]
Ions detection in water	Cu^{2+}	[30]
	tetra-n-butylammonium bromide (TBAB)	[35]
	Iron(III) ($Fe_{(III)}$)	[41]
	bacterial toxins	[48]
	Nickel ions (Ni^{2+})	[51]
	Cerium(III) ions ($Ce_{(III)}$)	[55]
	Pb(II) in contaminated water tests ($Pb_{(II)}$)	[57]
Ions detection in soil	K^+	[33]
	2-naphthoic acid	[45]
Analysis in agrifood and industry	Sulfite Ions in beverages (SO_3^{2-})	[29]
	K^+	[32]
	Cr(III) in the form of CrO_4^{2-} ($Cr_{(III)}$)	[39]
	Ca^{2+}	[42]
	H^+ (pH sensor)	[46]
	Diquat Herbicide (DQ)	[49]

VI. APPLICATIONS

ASS-ISEs are applied in a variety of fields, starting from medicine and extending to industry and agriculture. The wide applications are due to the great flexibility that ISEs have. There are examples in the literature of ASS-ISEs that actually evaluate not only individual ions [29], [30], [51], but they can also monitor entire molecules or drugs [25], [26], [50], [53], [54]. As can be seen from Table X, the applications are divided into five different groups with the idea of promoting the major macro areas in which ASS-ISE can be exploited to date.

A. Drugs and Molecules Monitoring for Healthcare

ASS-ISEs have created a new and promising field in pharmaceutical and biological analysis. They are recognized as an energy-saving, simple, and environmentally friendly measurement devices; in fact, all researchers want to help safeguard and improve the economy and the environment by discovering unique ways to reduce waste and find substitutes for hazardous chemicals.

Much of the literature concerns the monitoring of drugs and molecules for healthcare. Among the most studied molecules are opioid derivatives, including pholcodine [28], a morphine-derived drug; codeine phosphate [53], an opioid analgesic that has become a major source of pain treatment for patients. In the latter case, the sensor offered advantages of high sensitivity and low detectability (down to 40 ng/mL), improved potential stability and durability (for at least six months), rapid response (<20 s for a 10^{-5} mol/L drug solution), high selectivity on many common associated species.

The study of opioids competes with antidepressants, as molecules such as fluoxetine, one of five drugs included in the category of selective serotonin reuptake inhibitors (SSRIs) and is mainly used to manage major depressive disorder (MDD) [25], [37]; desvenlafaxine, an antidepressant

belonging to a class of drugs known as selective serotonin and norepinephrine reuptake inhibitors (SNRIs) [26]; clomipramine [44]; and fluvoxamine (FLV) [36], have been monitored. Again, it is shown that the proposed sensor has high sensitivity with a detection limit of 4.8×10^{-6} mol/L with a near-Nernstian cation slope of 55.0 ± 0.8 mV/decade ($r2 = 0.999$) and excellent selectivity in the presence of different species. In addition, MWCNTs have been used to reduce potential drift and resistance (R) and increase potential stability, bilayer, and geometrical capabilities. In addition, the use of the proposed sensor for FLV determination in different pharmaceutical and biological samples showed high recoveries and confirmed the validity of the proposed sensor for FLV determination in different samples.

El-Hanboushy et al. [50] evaluated in the literature the usefulness of antihypertensive drugs not only for the treatment of heart failure but also for liver and kidney disease. Additionally, Magdy et al. [54] monitored the molecule of chlorhexidine, a disinfectant found in a variety of products. Further research performed by Rizk et al. [52] was for tolperisone, a drug that belongs to the group of centrally acting muscle relaxants and is prescribed for the symptomatic treatment of spasticity, muscle spasms, and osteoarthritis. Other drugs monitored were caffeine (psychoactive drug) [27] and chlorpromazine (CPZ, antipsychotic drug). This sensor showed excellent capability for CPZ determination (LOD: 0.02 μM; linear concentration ranges from 0.02 to 172.74 and 222.48 to 1047.74 μM); high stability of operation and storage, RPR and RP, and excellent selectivity toward CPZ in the presence of other potentially interfering species. In addition, the practicality of the proposed sensor for CPZ detection was demonstrated by the analysis of real samples. Derar and Hussien [43] studied daclatasvir, a highly selective inhibitor for the viral enzyme that is responsible for hepatitis C virus replication. Here, the proposed electrode showed high sensitivity (Nernstian slope of 31.0 ± 1 mV/decade), a lower detection limit (8.5×10^{-7} M), and a wide linear range (1×10^{-5}–1×10^{-5}) compared with the PVC membrane without MWCNTs. In addition, the electrode demonstrates high potential stability with a potential drift of just 0.23 μV/min for 70 min after 10 min of preconditioning.

B. Ion Detection in Bio-Fluids

At the bio-fluid level, incorporating biochemical sensors into wearable platforms poses complex challenges. Access to biological fluids, such as blood and interstitial fluid, is usually avoided, as the skin barrier must be crossed to access the specimen, leading to wearer comfort issues and potential infection. For this reason, ASS-ISEs often adopt the so-called "spiked" fluids [59], [62], to reduce interference from all complex fluids and improve performance for sensor measurement. In contrast, in many ASS-ISEs, a different approach is adopted; sweat [31], [34], [47], [58] represents an easily accessible biological fluid, the composition of which includes electrolytes and metabolites that can provide information about an individual's health status and physical condition. Studies on additional biological fluids are also, nevertheless, noted, including urine [59] and serum [40]. In particular, cations and not anions are detected, including sodium [31], [34], [47], [59], [62], potassium [34], [58], [59], and ammonium [31]. Usually, sodium and potassium are studied for monitoring sweat, although Zamarayeva et al. [31] studied ammonium ions in sweat, while Kucherenko et al. [86] studied them in urine. Urine is usually studied to monitor hydration in patients, including those of advanced age. Ruecha et al. [59] monitored sodium ions and potassium ions not in sweat but in urine. Very special is the case of Bauer et al. [65], who monitored potassium ions not only in sweat but also in artificial tears, unlike Zuliani et al. [62], who studied sodium ions in real saliva samples. Human serum samples were considered for monitoring acetylcholine neurotransmitter and acetylcholinesterase enzyme activity [40]. The latter study demonstrates that PEDOT/PSS has excellent conductivity when used as an ion-electron transducer on PVC as a polymer matrix. Kamel et al. [38] monitored sodium deoxycholate as a bile salt in bovine serum albumin samples. Sodium deoxycholate is considered one of the salts of bile acids that are biosynthesized in the liver of the human body from the cholesterol fraction. The sensors fabricated for the study showed high sensitivity that reached a slope of 4.7×10^{-5} M near Nernestian [-60.1 ± 0.9 mV/decade, $r2 = 0.999$ ($n = 5$)]. The sensors revealed high selectivity, long lifetime, high potential stability, and conductivity to ensure reproducible and accurate results over a long period.

Some authors show the advantages of ASS-ISEs for potassium detection as they highlight the ability to print graphene on flexible, curvilinear surfaces, as well as the ability to detect potassium concentrations present in sweat. This implies that K^+-ISEs could also be suitable for wearable epidermal sensors that monitor potassium levels from eccrine sweat glands. This type of sensor appears to be low-cost for monitoring potassium in a variety of biomedical and environmental applications [58].

C. Environmental Monitoring

Environmental monitoring in the study of ASS-ISEs assumes a great deal of pollution control, so it allows feedback on water and soil quality to improve the surrounding environment.

Many analyses with ASS-ISEs for monitoring ions or molecules have been performed by studying water or soil. For water, interesting examples of monitoring nickel ions [51] or copper [30] have been presented by exploiting potentiometric sensors. Mostly, tap water is considered, but in some cases, water in the presence of petroleum also for Fe (II) [41] or cerium (III) [55] monitoring, or contaminated water for Pb (II) monitoring [57]. There are elite cases in water monitoring, including Queirós et al. [48], who monitored bacterial toxins, and Elashery et al. [35] tetra-n-butylammonium bromide (TBAB) in pure and spiked tap water samples [35]. These types of sensors showed a rapid, stable, reproducible, and selective response for TBAB over a wide and perceptible concentration range. Analytical applications of the sensors confirm that they hold promise for continuous and routine analysis of TBAB in various samples.

The use of ASS-ISEs can also be relevant for the evaluation of water quality efficiency in relation to public health. The World Health Organization (WHO) has established a guideline

for the use of various toxic substances (e.g., lead, zinc, arsenic, etc.) in drinking water, as they have been shown to cause serious diseases (e.g., cancer, children's development delays, fatal intoxication) or even mortality if present above standard levels [92], [93]. In this picture, the use of ASS-ISEs can be particularly relevant since their use can help to reduce the LOD facilitating a prompt identification of risky situations. In addition, the possibility of miniaturizing them and spreading them can help in performing capillary monitoring. Examples of studies with ASS-ISEs performed with this aim can be found in [48] and [57] where, respectively, bacterial toxins and lead ions are monitored within drinkable water exploiting SPE, or in [94] where ASS electrodes are exploited to realize a complete taste sensor to evaluate qualitatively and quantitatively selected samples of drinkable waters.

In addition to water quality assessment, soil monitoring studies also represent a relevant application to prevent the diffusion of pollutants and harmful and chemical substances. Relevant examples of ASS-ISEs used for soil monitoring can be found in [84], where ammonium and nitrate ions were monitored, and also in [33], where potassium ions were quantified. In this latest analysis, Rosenberg et al. [33] coupled the technology with a mobile phone-based fertilizer recommendation computer system that could enable low-cost soil testing and nutrient management for rural farmers worldwide.

Another example of industrial use at the soil level was studied by Li et al. [45] to monitor 2-naphthoic acid, the first decomposition product of naphthalene. Compared with the classical potentiometric sensor, the proposed sensor, based on a nonequilibrium sensing mechanism, shows greatly improved sensitivity for the detection of 2-naphthoic acid with a low detection limit of 6.91011 M.

D. Analysis in Agrifood and Industry

ASS-ISEs are used in monitoring the industrial and agrifood processes, as metals or pollutants are often present in food [32], [49], or beverages [29], [32], [49]. ASS-ISEs have several advantages within the industry as they reveal high sensitivity and selectivity for potentiometric monitoring of particular molecules and ions, low-cost instrumentation, no sample pretreatment required, and ease of operation. They also possess much flexibility in the field of food and beverages as well since several studies have succeeded in discriminating ions within solutions or even performing taste-type tests in appropriate solutions by testing the sensor in acidic, sour, and sweet solutions by discriminating different types of soft drinks [95]. Some molecules or ions considered are benign [35] and some are nonbiodegradable [51]. These elements can enter the food chain (meat, chocolate, hydrogenated and unsaturated oils, cornmeal, cottonseed, dairy products, preserved foods) and drinking or tap water and cause adverse health effects.

Hassan et al. [39], who studied metallic chromium present in the environment in trivalent and hexavalent ionic forms, made an example of a purely industrial-level study. Occupational exposure to chromium occurs in chromate processing, stainless steel production, chromium plating, and the tanning industry; thus, it is very toxic to humans, especially Cr (III) [39]. Zhang et al. [46], inherent to dyeing liquor monitoring through pH-selective sensors, did a particular study related to the textile industry. In this case, additional advantages were found in the pH-based PVC membrane type in that, in addition to its miniaturization and maintenance-free operation, it was pressure and heat-resistant, i.e., a big advantage over the fragile electrode traditional and fragile glassy electrode. This means that it has potential application in some special fields such as industry, biopharmaceutical analysis, and also biophysics [46].

Ions such as sulfites [29] and potassium [32] have been monitored in beverages. For the inherent potassium study, sensor types based on the RGO SC electrode have demonstrated high sensitivity, low detection limit, fast response time, and good selectivity compared with the bare Au electrode, improved potential stability, and more effectively prevented the formation of a water layer and light and gas interference. In addition, the potentiometric K^+ sensor made accurate measurements of K^+ concentration in real samples of sports drinks, coke, and orange juice, consistent with an electrochemical analyzer. It can, therefore, be said that SC RGO-based potentiometric ion sensors hold promise for reliable and reproducible electrochemical performance compared with solid-state ion sensors [32].

One particular study was conducted by Kamel et al. [49], who monitored the diquat content in commercial pesticide preparations and different spiked potato samples. Diquat is one of the most widely used herbicides. It is used for aquatic weed control and preharvest desiccation of potatoes, carrots, onions, vines, etc., and of seed crops (including rice, peas, clover, canola, beans, corn, etc.

VII. Discussion and Conclusion

Analysis of the articles included in this review identified the various materials used in the fabrication of solid-state ASS-ISEs, as well as limitations and shortcomings in process validation and printing procedures. In the literature, there is a lack of uniformity and standardization in the terminology adopted for the various metrological parameters and a mismatch with IUPAC guidance, which is useful for device characterization. Even if most of the articles analyzed the report in a uniform way regarding sensitivity, LOD, and linearity, other relevant performance metrics are missing or not homogeneously computed, particularly about selectivity, response time, RP, RPR, stability, and accuracy. After deeply analyzing the articles and comparing the computation of these metrics with the standard methods suggested by IUPAC, several recommendations can be provided to researchers dealing with printed ASS-ISE characterization. Selectivity is recommended to be calculated always relying on quantitative selectivity coefficients and not qualitatively since it would prevent the possibility of effectively comparing different sensors. In addition to the coefficient, it should indicate both the method (SSM or FIM), the concentration of the interferents, and the setup conditions. Response time should be measured, in agreement with the indication of IUPAC [91], as the time required to obtain a stable signal when the sensor is undergoing a specific concentration spike with a steady state value within 1 mV. To correctly evaluate this number, it is of foremost importance to detail the setup exploited for the

measurements regarding the volume of solution, the velocity of stirring, or the sample flowing on top of the electrodes. For RP and RPR, the most useful and rigorous method appears to be the one that takes into consideration replicated measurements performed, respectively, with the same or with different setups during the same timeframe, leaving the time variable for consideration in the stability metrics. Regarding stability, to provide a meaningful value, it should be indicated as a time (days, weeks, or months) along with the maximum drift, which is accepted to define the sensor's stability; furthermore, to avoid confusion, it should be clearly distinguished between short-term stability, the result of the water layer test, and long-term stability, providing along with the quantitative result also the conditions in which the sensors are maintained during the long-term testing. Finally, accuracy, which was not clearly stated in most of the articles, should be added in a standard characterization as the percentage of maximum divergence from the actual most reliable traditionally accepted laboratory equipment. This represents, in fact, a crucial value that could state if any novel ASS-ISE can compete with already existing methodologies.

The possibility enabled by novel deposition techniques enlarges the options regarding ink composition, allowing high-performance printing of also very thick inks with a higher loading [96]. The higher control and finer resolution that can be obtained, furthermore, by direct printing even of the membrane, seems to be printed only in a few cases [41], [43], [55], [57], [59]. These novel printing techniques could also help in making a step ahead in obtaining fully printed devices, not limiting the printing to the electrodes, but providing a fully printable device from substrate to sensitive membrane with properly customized inks [55]; therefore, these novel printing techniques could lead to improvements in the fabrication methods that could lead to improvements in the metrological characteristics. A first possible improvement of the sensitivity could be obtained by combining a micro-structuration with nanostructures, thus increasing the surface-to-volume ratio of the layer and consequently the area available for the exchange with the membrane [1], [97]. A second possible improvement could be related to the possibility of going beyond 2-D surfaces and printing on 3-D objects. In particular, thinking of wearable devices or specific probes for soil or water sensing, having all the layers printed on top of a surface that conforms to the surface under test could increase the interface area thus improving sensitivity to the target ions produced by the object under test [23]. Regarding membranes, different aspects of high-resolution printing techniques processes could improve their selectivity, reversibility, and stability, essential properties to obtain sensitivities near the ideal value [24]. From one side, the possibility of controlling temperature and pressure during the printing phase in techniques such as aerosol jet printing (AJP), nano-jet printing, or nano-dispensing could help to maximize the control of the physical parameters that the membrane is undergoing. Fine control over the geometry and the thickness can, furthermore, help to optimize membrane deposition to maximize the interface with the interlayer, even exploiting novel plasticizers alternative to the traditional PVC ones [98].

Despite these advantages, to date, there are still measurement issues related to uncertainties that do not allow intensive and exclusive use as the gold standard of these sensors. Indeed, monitoring of molecules and drugs, detection of ions or molecules in biofluids, the environment, industry, and agrifood has not yet been done through these methods to date, but other validated methods are more reliable, reproducible, and sensitive. In addition to this, there seems to be a lack of study in the literature on new geometries to be applied to both the interface material and the ISM. These geometries, as discussed earlier, can strongly affect the efficiency of the material used, and thus, can represent a crucial space for improvement. In conclusion, the printing techniques and the materials of use for each of the layers of the ASS-ISEs should be improved so as to enhance the sensitivity, selectivity, and especially the RPR of these sensors, which to date is somewhat lacking, so that they can be used in the future as portable devices in the health field and can be improved on the dimensions of current devices for water or soil monitoring.

REFERENCES

[1] T. Fapanni, E. Sardini, M. Serpelloni, and S. Tonello, "Nano-functionalized electrochemical sensors by aerosol jet printing," *IEEE Sensors J.*, vol. 22, no. 22, pp. 21498–21507, Nov. 2022, doi: 10.1109/JSEN.2022.3213349.

[2] R. Kalidoss, A. S. Raja, D. Jeyakumar, and N. Prabu, "Solid-state planar reference electrode with ion-selective electrodes for clinical diagnosis," *IEEE Sensors J.*, vol. 18, no. 20, pp. 8510–8516, Oct. 2018, doi: 10.1109/JSEN.2018.2865726.

[3] H. Karimi-Maleh et al., "A critical review on the use of potentiometric based biosensors for biomarkers detection," *Biosensors Bioelectron.*, vol. 184, Jul. 2021, Art. no. 113252, doi: 10.1016/j.bios.2021.113252.

[4] N. ElBeheiry and R. S. Balog, "Technologies driving the shift to smart farming: A review," *IEEE Sensors J.*, vol. 23, no. 3, pp. 1752–1769, Feb. 2023, doi: 10.1109/JSEN.2022.3225183.

[5] G. Lisak, "Reliable environmental trace heavy metal analysis with potentiometric ion sensors–reality or a distant dream," *Environ. Pollut.*, vol. 289, Nov. 2021, Art. no. 117882, doi: 10.1016/j.envpol.2021.117882.

[6] K. K. Yeung, T. Huang, Y. Hua, K. Zhang, M. M. F. Yuen, and Z. Gao, "Recent advances in electrochemical sensors for wearable sweat monitoring: A review," *IEEE Sensors J.*, vol. 21, no. 13, pp. 14522–14539, Jul. 2021, doi: 10.1109/JSEN.2021.3074311.

[7] J. Zhai, B. Luo, A. Li, H. Dong, X. Jin, and X. Wang, "Unlocking all-solid ion selective electrodes: Prospects in crop detection," *Sensors*, vol. 22, no. 15, p. 5541, Jul. 2022, doi: 10.3390/s22155541.

[8] A. la Grasta, M. De Carlo, A. Di Nisio, F. Dell'Olio, and V. M. N. Passaro, "Potentiometric chloride ion biosensor for cystic fibrosis diagnosis and management: Modeling and design," *Sensors*, vol. 23, no. 5, p. 2491, Feb. 2023, doi: 10.3390/s23052491.

[9] A. M. Benoudjit, I. U. S. Shohibuddin, M. M. Bader, and W. W. A. W. Salim, "Components of all-solid-state ion-selective electrodes (AS-ISEs)," in *Composite Materials: Applications in Engineering, Biomedicine and Food Science*, S. Siddiquee, M. G. J. Hong, and M. M. Rahman, Eds. Cham, Switzerland: Springer, 2020, pp. 351–366, doi: 10.1007/978-3-030-45489-0_16.

[10] M. Sohail and R. De Marco, "ELECTRODES | Ion-selective electrodes," in *Reference Module in Chemistry, Molecular Sciences and Chemical Engineering*. Amsterdam, The Netherlands: Elsevier, 2013, doi: 10.1016/B978-0-12-409547-2.01180-X.

[11] F. Criscuolo, M. I. N. Hanitra, I. Taurino, S. Carrara, and G. De Micheli, "All-solid-state ion-selective electrodes: A tutorial for correct practice," *IEEE Sensors J.*, vol. 21, no. 20, pp. 22143–22154, Oct. 2021, doi: 10.1109/JSEN.2021.3099209.

[12] M. R. Tamara, D. Lelono, R. Roto, and K. Triyana, "All-solid-state astringent taste sensor using polypyrrole-carbon black composite as ion-electron transducer," *Sens. Actuators A, Phys.*, vol. 351, Mar. 2023, Art. no. 114170, doi: 10.1016/j.sna.2023.114170.

[13] A. Moudgil, K. Hou, T. Li, and W. L. Leong, "Biocompatible solid-state ion-sensitive organic electrochemical transistor for physiological multi-ions sensing," *Adv. Mater. Technol.*, vol. 8, no. 18, Sep. 2023, Art. no. 2300605, doi: 10.1002/admt.202300605.

[14] M. S. Sumitha and T. S. Xavier, "Recent advances in electrochemical biosensors—A brief review," *Hybrid Adv.*, vol. 2, Apr. 2023, Art. no. 100023, doi: 10.1016/j.hybadv.2023.100023.

[15] K. Theyagarajan and Y.-J. Kim, "Recent developments in the design and fabrication of electrochemical biosensors using functional materials and molecules," *Biosensors*, vol. 13, no. 4, p. 424, Mar. 2023, doi: 10.3390/bios13040424.

[16] M. M. Shanbhag, G. Manasa, R. J. Mascarenhas, K. Mondal, and N. P. Shetti, "Fundamentals of bio-electrochemical sensing," *Chem. Eng. J. Adv.*, vol. 16, Nov. 2023, Art. no. 100516, doi: 10.1016/j.ceja.2023.100516.

[17] S. Cao et al., "ISFET-based sensors for (bio)chemical applications: A review," *Electrochem. Sci. Adv.*, vol. 3, no. 4, pp. 1–25, Aug. 2023, doi: 10.1002/elsa.202100207.

[18] X. Ma, R. Peng, W. Mao, Y. Lin, and H. Yu, "Recent advances in ion-sensitive field-effect transistors for biosensing applications," *Electrochem. Sci. Adv.*, vol. 3, no. 3, pp. 1–20, Jun. 2023, doi: 10.1002/elsa.202100163.

[19] N. Moser, T. S. Lande, C. Toumazou, and P. Georgiou, "ISFETs in CMOS and emergent trends in instrumentation: A review," *IEEE Sensors J.*, vol. 16, no. 17, pp. 6496–6514, Sep. 2016, doi: 10.1109/JSEN.2016.2585920.

[20] Y. Shao, Y. Ying, and J. Ping, "Recent advances in solid-contact ion-selective electrodes: Functional materials, transduction mechanisms, and development trends," *Chem. Soc. Rev.*, vol. 49, no. 13, pp. 4405–4465, Jul. 2020, doi: 10.1039/c9cs00587k.

[21] E. Sardini, M. Serpelloni, and S. Tonello, "Printed electrochemical biosensors: Opportunities and metrological challenges," *Biosensors*, vol. 10, no. 11, p. 166, Nov. 2020, doi: 10.3390/bios10110166.

[22] H. Jiang et al., "Inkjet-printed solid-state potentiometric nitrate ion selective electrodes for agricultural application," in *Proc. IEEE SENSORS*, Oct. 2019, pp. 1–4, doi: 10.1109/SENSORS43011.2019.8956650.

[23] P. Bellitti, M. Borghetti, E. Cantú, E. Sardini, and M. Serpelloni, "Resistive sensors for smart objects: Analysis on printing techniques," *IEEE Trans. Instrum. Meas.*, vol. 71, pp. 1–15, 2022, doi: 10.1109/TIM.2022.3181941.

[24] D. L. Glasco, N. H. B. Ho, A. M. Mamaril, and J. G. Bell, "3D printed ion-selective membranes and their translation into point-of-care sensors," *Anal. Chem.*, vol. 93, no. 48, pp. 15826–15831, Dec. 2021, doi: 10.1021/acs.analchem.1c03762.

[25] H. S. M. Abd-Rabboh et al., "All-solid-state potentiometric platforms modified with a multi-walled carbon nanotubes for fluoxetine determination," *Membranes*, vol. 12, no. 5, p. 446, Apr. 2022, doi: 10.3390/membranes12050446.

[26] M. A. Bajaber and A. H. Kamel, "All-solid state potentiometric sensors for desvenlafaxine detection using biomimetic imprinted polymers as recognition receptors," *Polymers*, vol. 14, no. 22, p. 4814, Nov. 2022, doi: 10.3390/polym14224814.

[27] H. S. M. Abd-Rabboh, A. E.-G. E. Amr, A. A. Almehizia, A. M. Naglah, and A. H. Kamel, "New potentiometric screen-printed platforms modified with reduced graphene oxide and based on man-made imprinted receptors for caffeine assessment," *Polymers*, vol. 14, no. 10, p. 1942, May 2022, doi: 10.3390/polym14101942.

[28] H. S. M. Abd-Rabboh, A. E.-G. E. Amr, A. A. Almehizia, and A. H. Kamel, "All-solid-state potentiometric ion-sensors based on tailored imprinted polymers for pholcodine determination," *Polymers*, vol. 13, no. 8, p. 1192, Apr. 2021, doi: 10.3390/polym13081192.

[29] H. S. M. Abd-Rabboh, A. E.-G.-E. Amr, A. H. Kamel, M. A. Al-Omar, and A. Y. A. Sayed, "Integrated all-solid-state sulfite sensors modified with two different ion-to-electron transducers: Rapid assessment of sulfite in beverages," *RSC Adv.*, vol. 11, no. 6, pp. 3783–3791, Jan. 2021, doi: 10.1039/d0ra09903a.

[30] J. Li and W. Qin, "An integrated all-solid-state screen-printed potentiometric sensor based on a three-dimensional self-assembled graphene aerogel," *Microchem. J.*, vol. 159, Dec. 2020, Art. no. 105453, doi: 10.1016/j.microc.2020.105453.

[31] A. M. Zamarayeva et al., "Optimization of printed sensors to monitor sodium, ammonium, and lactate in sweat," *APL Mater.*, vol. 8, no. 10, Oct. 2020, Art. no. 100905, doi: 10.1063/5.0014836.

[32] J. H. Yoon, H. J. Park, S. H. Park, K. G. Lee, and B. G. Choi, "Electrochemical characterization of reduced graphene oxide as an ion-to-electron transducer and application of screen-printed all-solid-state potassium ion sensors," *Carbon Lett.*, vol. 30, no. 1, pp. 73–80, Feb. 2020, doi: 10.1007/s42823-019-00072-6.

[33] R. Rosenberg, M. S. Bono, S. Braganza, C. Vaishnav, R. Karnik, and A. J. Hart, "In-field determination of soil ion content using a handheld device and screen-printed solid-state ion-selective electrodes," *PLoS ONE*, vol. 13, no. 9, Sep. 2018, Art. no. e0203862, doi: 10.1371/journal.pone.0203862.

[34] P. Pirovano et al., "A wearable sensor for the detection of sodium and potassium in human sweat during exercise," *Talanta*, vol. 219, Nov. 2020, Art. no. 121145, doi: 10.1016/j.talanta.2020.121145.

[35] S. E. A. Elashery, E. Y. Frag, and M. G. Mousa, "A comparative study of tetra-*n*-butylammonium bromide potentiometric selective screen printed, carbon paste and carbon nanotube modified graphite sensors," *J. Iranian Chem. Soc.*, vol. 17, no. 4, pp. 911–921, Apr. 2020, doi: 10.1007/s13738-019-01825-w.

[36] H. M. Hashem, S. S. M. Hassan, A. H. Kamel, A. E.-G. E. Amr, and E. M. AbdelBary, "Cost-effective potentiometric platforms modified with multi-walled carbon nanotubes (MWCNTs) and based on imprinted receptors for fluvoxamine assessment," *Polymers*, vol. 12, no. 3, p. 673, Mar. 2020.

[37] S. S. M. Hassan, A. H. Kamel, A. E.-G.-E. Amr, H. M. Hashem, and E. M. A. Bary, "Imprinted polymeric beads-based screen-printed potentiometric platforms modified with multi-walled carbon nanotubes (MWCNTs) for selective recognition of fluoxetine," *Nanomaterials*, vol. 10, no. 3, p. 572, Mar. 2020.

[38] A. H. Kamel, S. Ezzat, M. A. Ahmed, A. E.-G.-E. Amr, A. A. Almehizia, and M. A. Al-Omar, "Modified potentiometric screen-printed electrodes based on imprinting character for sodium deoxycholate determination," *Biomolecules*, vol. 10, no. 2, p. 251, Feb. 2020, doi: 10.3390/biom10020251.

[39] S. S. M. Hassan, A. H. Kamel, A. E.-G.-E. Amr, M. Abdelwahab Fathy, and M. A. Al-Omar, "Paper strip and ceramic potentiometric platforms modified with nano-sized polyaniline (PANi) for static and hydrodynamic monitoring of chromium in industrial samples," *Molecules*, vol. 25, no. 3, p. 629, Jan. 2020, doi: 10.3390/molecules25030629.

[40] N. H. Ashmawy, A. A. Almehizia, T. A. Youssef, A. E. G. E. Amr, M. A. Al-Omar, and A. H. Kamel, "Novel carbon/PEDOT/PSS-based screen-printed biosensors for acetylcholine neurotransmitter and acetylcholinesterase detection in human serum," *Molecules*, vol. 24, no. 8, p. 1539, Apr. 2019, doi: 10.3390/molecules24081539.

[41] T. A. Ali, G. G. Mohamed, H. Eldessouky, and A.-E. Adeeb, "Ion selective electrodes based on methyl 6-(hydroxymethyl) picolinate ionophore for electrochemical determination of Fe(III) in petroleum water samples," *Egyptian J. Petroleum*, vol. 28, no. 2, pp. 233–239, Jun. 2019, doi: 10.1016/j.ejpe.2019.04.002.

[42] C. Ocaña, N. Abramova, A. Bratov, T. Lindfors, and J. Bobacka, "Calcium-selective electrodes based on photo-cured polyurethane-acrylate membranes covalently attached to methacrylate functionalized poly(3,4-ethylenedioxythiophene) as solid-contact," *Talanta*, vol. 186, pp. 279–285, Aug. 2018, doi: 10.1016/j.talanta.2018.04.056.

[43] A. R. Derar and E. M. Hussien, "Disposable multiwall carbon nanotubes based screen printed electrochemical sensor with improved sensitivity for the assay of daclatasvir: Hepatitis C antiviral drug," *IEEE Sensors J.*, vol. 19, no. 5, pp. 1626–1632, Mar. 2019, doi: 10.1109/JSEN.2018.2883656.

[44] A. M. Michael, A. M. Mahmoud, and N. M. Fahmy, "Determination of clomipramine using eco-friendly solid-contact ionophore-doped potentiometric sensor," *BMC Chem.*, vol. 17, no. 1, pp. 1–9, Mar. 2023, doi: 10.1186/s13065-023-00938-x.

[45] P. Li, R. Liang, X. Yang, and W. Qin, "Imprinted nanobead-based disposable screen-printed potentiometric sensor for highly sensitive detection of 2-naphthoic acid," *Mater. Lett.*, vol. 225, pp. 138–141, Aug. 2018, doi: 10.1016/j.matlet.2018.04.119.

[46] J. Zhang, Y. Guo, S. Li, and H. Xu, "A solid-contact pH-selective electrode based on tridodecylamine as hydrogen neutral ionophore," *Meas. Sci. Technol.*, vol. 27, no. 10, Oct. 2016, Art. no. 105101, doi: 10.1088/0957-0233/27/10/105101.

[47] G. Matzeu et al., "An integrated sensing and wireless communications platform for sensing sodium in sweat," *Anal. Methods*, vol. 8, no. 1, pp. 64–71, 2016, doi: 10.1039/c5ay02254a.

[48] R. B. Queirós, A. Guedes, P. V. S. Marques, J. P. Noronha, and M. G. F. Sales, "Recycling old screen-printed electrodes with newly designed plastic antibodies on the wall of carbon nanotubes as sensory element for in situ detection of bacterial toxins in water," *Sens. Actuators B, Chem.*, vol. 189, pp. 21–29, Dec. 2013, doi: 10.1016/j.snb.2012.11.112.

[49] A. H. Kamel, A. E.-G.-E. Amr, N. S. Abdalla, M. El-Naggar, M. A. Al-Omar, and A. A. Almehizia, "Modified screen-printed potentiometric sensors based on man-tailored biomimetics for diquat herbicide determination," *Int. J. Environ. Res. Public Health*, vol. 17, no. 4, p. 1138, Feb. 2020, doi: 10.3390/ijerph17041138.

[50] S. El-Hanboushy, A. M. Mahmoud, Y. M. Fayez, H. M. Lotfy, M. Abdelkawy, and H. M. Marzouk, "Design of green polypyrrole-based solid-contact ion-selective sensors for determination of antihypertensive drugs in combined dosage forms and spiked human plasma," *J. Electrochem. Soc.*, vol. 170, no. 3, Mar. 2023, Art. no. 037520, doi: 10.1149/1945-7111/acc361.

[51] A. Darroudi, "Electrophoretic deposition of graphene oxide on screen-imprinted carbon electrode and its modification using Ni^{2+}-imprinted polymer as ionophere by a potentiometric sensor for determination of nickel ions," *Anal. Bioanal. Chem. Res.*, vol. 10, no. 1, pp. 63–70, 2023. [Online]. Available: http://www.analchemres.org/article_158794.html

[52] M. Rizk, E. M. Hussein, S. Toubar, E. Ramzy, and M. I. Helmy, "Screen-printed sensors for efficient potentiometric analysis of tolperisone hydrochloride in presence of its co-formulated drugs," *BMC Chem.*, vol. 16, no. 1, pp. 1–10, Nov. 2022, doi: 10.1186/s13065-022-00883-1.

[53] S. S. M. Hassan, A. H. Kamel, and M. A. Fathy, "A novel screen-printed potentiometric electrode with carbon nanotubes/polyaniline transducer and molecularly imprinted polymer for the determination of nalbuphine in pharmaceuticals and biological fluids," *Analytica Chim. Acta*, vol. 1227, Sep. 2022, Art. no. 340239, doi: 10.1016/j.aca.2022.340239.

[54] N. Magdy, A. E. Sobaih, L. A. Hussein, and A. M. Mahmoud, "Graphene-based disposable electrochemical sensor for chlorhexidine determination," *Electroanalysis*, vol. 35, no. 2, Feb. 2023, Art. no. e202200119, doi: 10.1002/elan.202200119.

[55] T. A. Ali and G. G. Mohamed, "Design and construction of an electrochemical sensor for the determination of cerium(III) ions in petroleum water samples based on a Schiff base-carbon nanotube as an ionophore," *RSC Adv.*, vol. 12, no. 1, pp. 94–103, Dec. 2021, doi: 10.1039/d1ra08337f.

[56] H. M. Essam, Y. F. Bassuoni, E. S. Elzanfaly, H. E.-S. Zaazaa, and K. M. Kelani, "Potentiometric sensing platform for selective determination and monitoring of codeine phosphate in presence of ibuprofen in pharmaceutical and biological matrices," *Microchem. J.*, vol. 159, Dec. 2020, Art. no. 105286, doi: 10.1016/j.microc.2020.105286.

[57] T. A. Ali, A. M. E. Hassan, and G. G. Mohamed, "Manufacture of lead-specific screen-printed sensor based on lead Schiff base complex as carrier and multi-walled carbon nanotubes for detection of Pb(II) in contaminated water tests," *Int. J. Electrochem. Sci.*, vol. 11, no. 12, pp. 10732–10747, Dec. 2016, doi: 10.20964/2016.12.30.

[58] Q. He et al., "Enabling inkjet printed graphene for ion selective electrodes with postprint thermal annealing," *ACS Appl. Mater. Interfaces*, vol. 9, no. 14, pp. 12719–12727, Apr. 2017, doi: 10.1021/acsami.7b00092.

[59] N. Ruecha, O. Chailapakul, K. Suzuki, and D. Citterio, "Fully inkjet-printed paper-based potentiometric ion-sensing devices," *Anal. Chem.*, vol. 89, no. 19, pp. 10608–10616, Oct. 2017, doi: 10.1021/acs.analchem.7b03177.

[60] A. Hussain, N. Abbas, and A. Ali, "Inkjet printing: A viable technology for biosensor fabrication," *Chemosensors*, vol. 10, no. 3, p. 103, Mar. 2022, doi: 10.3390/chemosensors10030103.

[61] A. García-Miranda Ferrari, S. J. Rowley-Neale, and C. E. Banks, "Screen-printed electrodes: Transitioning the laboratory in-to-the field," *Talanta Open*, vol. 3, Aug. 2021, Art. no. 100032, doi: 10.1016/j.talo.2021.100032.

[62] C. Zuliani, G. Matzeu, and D. Diamond, "A liquid-junction-free reference electrode based on a PEDOT solid-contact and ionogel capping membrane," *Talanta*, vol. 125, pp. 58–64, Jul. 2014, doi: 10.1016/j.talanta.2014.02.018.

[63] A. K. S. Kumar, Y. Zhang, D. Li, and R. G. Compton, "A mini-review: How reliable is the drop casting technique?" *Electrochem. Commun.*, vol. 121, Dec. 2020, Art. no. 106867, doi: 10.1016/j.elecom.2020.106867.

[64] N. Sebastian, W.-C. Yu, Y.-C. Hu, D. Balram, and Y.-H. Yu, "Sonochemical synthesis of iron-graphene oxide/honeycomb-like ZnO ternary nanohybrids for sensitive electrochemical detection of antipsychotic drug chlorpromazine," *Ultrason. Sonochem.*, vol. 59, Dec. 2019, Art. no. 104696, doi: 10.1016/j.ultsonch.2019.104696.

[65] M. Bauer et al., "Electrochemical multi-analyte point-of-care perspiration sensors using on-chip three-dimensional graphene electrodes," *Anal. Bioanal. Chem.*, vol. 413, no. 3, pp. 763–777, Jan. 2021, doi: 10.1007/s00216-020-02939-4.

[66] H. S. M. Abd-Rabboh, A. El-Galil E. Amr, E. A. Elsayed, A. Y. A. Sayed, and A. H. Kamel, "Paper-based potentiometric sensing devices modified with chemically reduced graphene oxide (CRGO) for trace level determination of pholcodine (opiate derivative drug)," *RSC Adv.*, vol. 11, no. 20, pp. 12227–12234, 2021, doi: 10.1039/d1ra00581b.

[67] E. Lindner and Y. Umezawa, "Performance evaluation criteria for preparation and measurement of macro- and microfabricated ion-selective electrodes (IUPAC technical report)," *Pure Appl. Chem.*, vol. 80, no. 1, pp. 85–104, Jan. 2008, doi: 10.1351/pac200880010085.

[68] K. Maksymiuk, E. Stelmach, and A. Michalska, "Unintended changes of ion-selective membranes composition—Origin and effect on analytical performance," *Membranes*, vol. 10, no. 10, p. 266, Sep. 2020, doi: 10.3390/membranes10100266.

[69] M. Rich et al., "Circumventing traditional conditioning protocols in polymer membrane-based ion-selective electrodes," *Anal. Chem.*, vol. 88, no. 17, pp. 8404–8408, Sep. 2016, doi: 10.1021/acs.analchem.6b01542.

[70] Z. Su, X. Ran, J. J. Leitch, A. L. Schwan, R. Faragher, and J. Lipkowski, "How valinomycin ionophores enter and transport K^+ across model lipid bilayer membranes," *Langmuir*, vol. 35, no. 51, pp. 16935–16943, Dec. 2019, doi: 10.1021/acs.langmuir.9b03064.

[71] N. Phan, H. Sussitz, and P. Lieberzeit, "Polymerization parameters influencing the QCM response characteristics of BSA MIP," *Biosensors*, vol. 4, no. 2, pp. 161–171, Jun. 2014, doi: 10.3390/bios4020161.

[72] H. E. K. Ertürün, A. D. Özel, M. N. Ayanoğlu, Ö. Şahin, and M. Yılmaz, "A calix[4]arene derivative-doped perchlorate-selective membrane electrodes with/without multi-walled carbon nanotubes," *Ionics*, vol. 23, no. 4, pp. 917–927, Apr. 2017, doi: 10.1007/s11581-016-1906-8.

[73] D. A. Armbruster and T. Pry, "Limit of blank, limit of detection and limit of quantitation," *Clin. Biochem. Rev.*, vol. 29, no. 1, pp. S49–S52, Aug. 2008.

[74] S. R. Shin et al., "Aptamer-based microfluidic electrochemical biosensor for monitoring cell-secreted trace cardiac biomarkers," *Anal. Chem.*, vol. 88, no. 20, pp. 10019–10027, Oct. 2016, doi: 10.1021/acs.analchem.6b02028.

[75] R. P. Buck and E. Lindner, "Recommendations for nomenclature of ionselective electrodes (IUPAC recommendations 1994)," *Pure Appl. Chem.*, vol. 66, no. 12, pp. 2527–2536, Jan. 1994, doi: 10.1351/pac199466122527.

[76] N. G. Di Novo, E. Cantú, S. Tonello, E. Sardini, and M. Serpelloni, "Support-material-free microfluidics on an electrochemical sensors platform by aerosol jet printing," *Sensors*, vol. 19, no. 8, p. 1842, Apr. 2019, doi: 10.3390/s19081842.

[77] M. Serpelloni, E. Cantú, M. Borghetti, and E. Sardini, "Printed smart devices on cellulose-based materials by means of aerosol-jet printing and photonic curing," *Sensors*, vol. 20, no. 3, p. 841, Feb. 2020, doi: 10.3390/s20030841.

[78] W.-J. Lan et al., "Paper-based potentiometric ion sensing," *Anal. Chem.*, vol. 86, no. 19, pp. 9548–9553, Oct. 2014, doi: 10.1021/ac5018088.

[79] E. Bakker and E. Pretsch, "Peer reviewed: The new wave of ion-selective electrodes," *Anal. Chem.*, vol. 74, no. 15, pp. 420 A–426 A, Aug. 2002, doi: 10.1021/ac022086f.

[80] J. G. Calvert, "Glossary of atmospheric chemistry terms (recommendations 1990)," *Pure Appl. Chem.*, vol. 62, no. 11, pp. 2167–2219, Jan. 1990, doi: 10.1351/pac199062112167.

[81] A. Golparvar, S. Tonello, A. Meimandi, and S. Carrara, "Inkjet-printed soft intelligent medical bracelet for simultaneous real-time sweat potassium (K^+), sodium (Na^+), and skin temperature analysis," *IEEE Sensors Lett.*, vol. 7, no. 5, pp. 1–4, May 2023, doi: 10.1109/LSENS.2023.3267180.

[82] S. Tonello, A. Golparvar, A. Meimandi, and S. Carrara, "Multimodal sweat ion and sweat rate sensing with inkjet-printed flexible bracelet and paperfluidics," in *Proc. IEEE Int. Symp. Med. Meas. Appl. (MeMeA)*, Jun. 2023, pp. 1–6, doi: 10.1109/MeMeA57477.2023.10171913.

[83] S. Søpstad, E. A. Johannessen, and K. Imenes, "Analytical errors in biosensors employing combined counter/pseudo-reference electrodes," *Results Chem.*, vol. 2, Jan. 2020, Art. no. 100028, doi: 10.1016/j.rechem.2020.100028.

[84] N. T. Garland et al., "Flexible laser-induced graphene for nitrogen sensing in soil," *ACS Appl. Mater. Interfaces*, vol. 10, no. 45, pp. 39124–39133, Nov. 2018, doi: 10.1021/acsami.8b10991.

[85] Y. Umezawa, P. Bühlmann, K. Umezawa, K. Tohda, and S. Amemiya, "Potentiometric selectivity coefficients of ion-selective electrodes. Part I. Inorganic cations (technical report)," *Pure Appl. Chem.*, vol. 72, no. 10, pp. 1851–2082, Jan. 2000, doi: 10.1351/pac200072101851.

[86] I. S. Kucherenko et al., "Ion-Selective sensors based on laser-induced graphene for evaluating human hydration levels using urine samples," *Adv. Mater. Technol.*, vol. 5, no. 6, pp. 1–9, Jun. 2020, doi: 10.1002/admt.201901037.

[87] E. Bakker, "Determination of improved selectivity coefficients of polymer membrane ion-selective electrodes by conditioning with a discriminated ion," *J. Electrochem. Soc.*, vol. 143, no. 4, pp. L83–L85, Apr. 1996, doi: 10.1149/1.1836608.

[88] B. G. Thiam, A. El Magri, H. R. Vanaei, and S. Vaudreuil, "3D printed and conventional membranes—A review," *Polymers*, vol. 14, no. 5, p. 1023, Mar. 2022, doi: 10.3390/polym14051023.

[89] I. Sadeghi, P. Kaner, and A. Asatekin, "Controlling and expanding the selectivity of filtration membranes," *Chem. Mater.*, vol. 30, no. 21, pp. 7328–7354, Nov. 2018, doi: 10.1021/acs.chemmater.8b03334.

[90] Y. Liu, X. Zeng, G. I. N. Waterhouse, X. Jiang, Z. Zhang, and L. Yu, "Potential stability improvement in Pb^{2+} ion selective electrodes by applying hydrophobic polyaniline as ion-to-electron transducer," *Synth. Met.*, vol. 281, Nov. 2021, Art. no. 116898, doi: 10.1016/j.synthmet.2021.116898.

[91] C. Maccà, "Response time of ion-selective electrodes," *Analytica Chim. Acta*, vol. 512, no. 2, pp. 183–190, Jun. 2004, doi: 10.1016/j.aca.2004.03.010.

[92] *Guidelines for Drinking-Water Quality*, 4th ed., WHO, Geneva, Switzerland, 2017.

[93] H. Barton, "Predicted intake of trace elements and minerals via household drinking water by 6-year-old children from Krakow, Poland. Part 5: Zinc," *Int. J. Prod. Res.*, vol. 23, no. 3, pp. 315–326, Sep. 2011.

[94] E. Marjanska and M. Szpakowska, "Qualitative and quantitative analysis of selected tonic waters by potentiometric taste sensor with all-solid-state electrodes," *IEEE Sensors J.*, vol. 18, no. 3, pp. 1250–1255, Feb. 2018, doi: 10.1109/JSEN.2017.2780283.

[95] M. Szpakowska, J. Szwacki, and E. Marjańska, "Multichannel taste sensors with lipid, lipid like—Polymer membranes," *J. Phys., Conf. Ser.*, vol. 127, Aug. 2008, Art. no. 012013, doi: 10.1088/1742-6596/127/1/012013.

[96] Y. Qin, A. U. Alam, M. M. R. Howlader, N. Hu, and M. J. Deen, "Inkjet printing of a highly loaded palladium ink for integrated, low-cost pH sensors," *Adv. Funct. Mater.*, vol. 26, no. 27, pp. 4923–4933, Jul. 2016, doi: 10.1002/adfm.201600657.

[97] T. Fapanni, E. Sardini, M. Serpelloni, and S. Tonello, "3D electrochemical sensor and microstructuration using aerosol jet printing," *Sensors*, vol. 21, no. 23, p. 7820, Nov. 2021, doi: 10.3390/s21237820.

[98] Á. Golcs, B. Vermes, D. C. Siwek, P. Huszthy, and T. Tóth, "Innovation in potentiometry: 3D-printed polylactic acid-based ion-selective bulk electrode membranes," *J. Appl. Electrochem.*, vol. 52, no. 9, pp. 1369–1382, Sep. 2022, doi: 10.1007/s10800-022-01706-w.

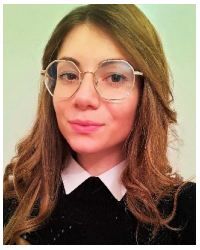

Giorgia Polidori received the M.S. (cum laude) degree in medical biotechnology, bioengineering curriculum, from the University of Rome, Rome, Italy, in 2023. She is currently pursuing the Ph.D. degree in technology for health with the University of Brescia, Brescia, Italy.

She is working on the electrochemical printed sensor for biotechnology applications. Her research interests include biosensors, tissue engineering, and regenerative medicine.

Sarah Tonello (Member, IEE) received the M.S. (cum laude) degree in biomedical engineering from the University of Florida, Gainesville, FL, USA, and the Politecnico di Milano, Milan, Italy, in 2014, as part of the dual degree program Atlantis CRISP, and the Ph.D. degree in technology for health from the University of Brescia, Brescia, Italy, in 2017.

She is currently a Researcher with the Department of Information Engineering, University of Padova, Padua, Italy. Her research interests include printed sensors, electronic devices, and electrochemical sensors.

Mauro Serpelloni (Senior Member, IEEE) received the M.S. (cum laude) degree in industrial management engineering and the Ph.D. degree in electronic instrumentation from the University of Brescia, Brescia, Italy, in 2003 and 2007, respectively.

He is currently a Full Professor with the Department of Information Engineering, University of Brescia. His current research interests include biomechatronic systems, contactless transmission, signal processing for microelectromechanical systems, and printed electronics.

Open Access funding provided by 'Università degli Studi di Brescia' within the CRUI-CARE Agreement